Stretching-Induced Foaming of Gas-Laden Thermoplastic Elastomers

Weiyuan Lin, Masahiro Ohshima

Department of Chemical Engineering, Kyoto University, Kyoto 615-8510, Japan

Abstract

Stretching-induced foaming of gas-laden thermoplastic elastomer (TPE), styrene-isobutylene-styrene (SIBS), was successfully conducted. CO_2-laden TPE plates were prepared by an injection molding process without foaming and later foamed by stretching. The effects of CO_2 concentration in the gas-laden elastomer, stretching rate (strain rate), and strain on bubble (cell) diameter and bubble density of the resulting foams were investigated, and a new bubble nucleation rate model was proposed to reflect the stretching effect on bubble nucleation in foam. The model has the stretching rate-dependent elastic strain energy in the bubble nucleation rate to explain why the higher stretching rate and the higher strain produce more bubbles of smaller size. The proposed bubble nucleation model clarifies the effect of the elastic modulus of TPE on the bubble nucleation barrier.

Keywords: Thermoplastic elastomer, Stretching-induced foaming, Bubble nucleation, Elastic strain energy

Introduction

As one of the promising technologies that has broadened the applications of various polymeric materials in recent decades, foaming has become an inevitable trend of polymer usage in industries [1] due to weight reduction, exceptional mechanical properties [2-3], and insulation (thermal and acoustic) properties [4-6]. Weight reduction leads to low consumption of materials and, thus, fuel savings and cost reduction [7]. Polymer foaming technology can be roughly divided into two methods: chemical and physical foaming. Whereas sustainable development and environmentally friendly life have been mainstream in today's society, physical foaming with green and harmless blowing agents has drawn more attention than chemical foaming. Although there are a variety of approaches to preparing polymer foams, the procedure can be concluded: formation of polymer/gas mixture, bubble nucleation induced by

thermodynamic instability (pressure drop or temperature increase), bubble growth, and solidification of cell structure.

It is well known that critical phenomena of physical foaming include bubble nucleation [8] and growth, which significantly affect the cell structure (bubble density and bubble diameter) of the foams. Several models simulating bubble nucleation and growth phenomena were proposed based on classic nucleation theory. However, the classic nucleation theory alone describes a thermodynamic process, which does not reflect the polymer nature, such as viscoelasticity and fluidity. It has not been sufficient to explain bubble nucleation in polymers, which creates a significant challenge for foaming researchers to consolidate and advance polymer-foaming technology. Han and Han considered the effect of shear stress to study bubble nucleation in a shear flow field [9]. They pointed out that bubble nucleation could be promoted by shear flow under unsaturation conditions with a physical blowing agent or flow of the material. Lee reported a modified cavity model to understand the enhancement effect of shear on bubble nucleation [10, 11]. He mentioned that shear was not only the dominant factor and that the melt temperature of the polymer also had a substantial impact on bubble nucleation. Based on the energy transformation from mechanical shear energy to surface energy, Chen and coworkers explained that shear stress promotes bubble nucleation [12]. Guo and Peng discussed the shear nucleation theory for microcellular foam extrusion processes. They elucidated that shear effects acted as a main driving force for bubble nucleation compared with the supersaturation in the microcellular foam extrusion [13]. Wong et al. investigated the effects of shear or extensional stress on bubble nucleation [14-17]. Wong et al. developed a visualization system for observing batch foaming phenomena in a view cell under shear or extensional stress. They concluded that shear or extensional stress played an essential role in enhancing bubble nucleation, and the reduction in local pressure induced by tensile stress could benefit bubble nucleation. In contrast, the increase in local pressure induced by compressive stress could hinder bubble nucleation. Wang et al. [18] identified the effect of elastic strain energy on bubble nucleation and successfully prepared submicrocellular TPU microfilms by stretching and compressing the samples before foaming. Their results showed that both compression and stretching were beneficial for enhancing bubble nucleation, but compression alone was not as effective as stretching because the energy barrier increased under compression. They proposed a bubble nucleation model in their supporting information, which augmented the elastic strain energy in the bubble nucleation rate equation to qualitatively explain the strain's effect on cell density. The effect of extensional stress on the bubble nucleation rate is

needed to investigate the pressure or temperature quenching effect independently. Our previous work also introduced an elastic strain energy function to the Gibbs free energy of the classical nucleation rate equation to reflect the elastic nature of the polymer [19]. The modified equation can apply to nanocellular foam and engineering plastic foam, where the elasticity of the polymer is high. However, it still has an ambiguity in the definition of the initial size of the bubble embryo and difficulty in dealing with the shear or strain rates.

This work used a kind of thermoplastic elastomer, styrene-isobutylene-styrene block copolymer (SIBS), as a base polymer. The elastic nature of SIBS provides uniform elongational deformation when it is stretched. Nonfoamed CO_2-laden SIBS was prepared by a foam injection molding machine with low gas delivery pressure and subsequently stretched by a tensile tester. Changing the strain and stretching rate of the tensile tester, the gas-laden SIBS was stretched, and the effects of stretching degree and rate, i.e., elastic strain energy and stretching rate, on bubble nucleation rate were investigated to separate the effects of pressure and temperature quenching. A bubble nucleation model including the elastic energy and stretching rate is proposed from the stretching-induced foaming cell structure.

2 Experimental

2.1 Materials

Two grades of styrene-isobutylene-styrene block copolymer (SIBS073T and SIBS062M, Kaneka, Osaka, Japan) were used as is. The melt flow rate, the number-average molecular weight, $\bar{M}_n$, and the weight-average molecular weights, $\bar{M}_W$, of SIBS073T are 6.0 g/10 min (230 ℃/2.16 kg), 58,000 and 81,000, respectively. Those of SIBS062M are 20.0 g/10 min (230 ℃/2.16 kg), 39,000 and 65,000. The ratio of the hard to soft segments are given in Supporting Information. Carbon dioxide (CO_2) of 99% purity (Izumi Sanyo, Tokyo, Japan) was utilized as a physical blowing agent (PBA).

2.2 Sample preparation and the stretching-induced foaming process

A foam injection molding (FIM) machine that does not need a high-pressure pumping system was employed to prepare the gas-laden TPE without foaming the product. Further details of the FIM can be found in our previous works [20, 21]. The FIM machine is a 35-ton clamping force electric injection molding machine, whose screw was 22 mm in diameter

(J35AD-AD30H, Japan Steel Work, Ltd. Japan). The mold has a rectangular cavity with dimensions of 40 mm × 10 mm × 2 mm. The cylinder temperatures were set as 40, 120, 180, 200, 200, 200, 200, and 200 ℃ from the feeding zone to the nozzle zone. The experimental conditions are summarized in Table 1 below.

Table 1 Experimental conditions for the low-pressure injection molding machine.

Parameters	Values
Gas type	CO_2
Gas pressure (MPa)	2, 3, 4, 5
Cylinder Temperature (℃)	40, 120, 180, 200, 200, 200, 200, 200
Mold temperature (℃)	30
Holding pressure (MPa)	30
Injection speed (mm/s)	20
Dwelling time (s)	6

Gas delivery pressure was kept below 5 MPa, to prevent the gas-laden samples from foaming in the injection molding process . After ejection of a nonfoamed but gas-laden molded sample, the sample was fixed to and stretched by a universal testing machine (Autograph AGS-1kN, Shimazu, Japan). Before fixing the sample to the tensile tester, the weight of each sample was measured, and its spur was cut out. Uniaxial stretching was conducted at different stretching rates of 50, 100, 200, and 400 mm/min. The final strain was also changed to three levels, 100, 200 and 300%.

2.3 Foam structure characterization

The cell structure, e.g., bubble density and bubble size, of the stretching-induced foams was evaluated using a scanning electron microscope (Tiny-SEM Mighty-8, Technex, Tokyo, Japan). A small slice specimen was cut from the center of the stretching-induced foam and cryogenically fractured in liquid nitrogen. The cross-sectional area was gold-coated using a quick coater (VPS-020, ULVAC KIKO, Ltd., Japan). Then, SEM images were analyzed using ImageJ (National Institutes of Health, USA). The number-average bubble diameter was calculated by Eq. (1) [22, 23]:

$$d = \frac{\Sigma d_i n_i}{\Sigma n_i} \qquad (1)$$

where n_i is the number of bubbles with a diameter of d_i. The bubble shape is assumed to be spherical. The bubble density (N_0) was calculated by Eq. (2) [21, 23]:

$$N_0 = \left(\frac{n}{A}\right)^{\frac{3}{2}} \qquad (2)$$

where n represents the total number of bubbles in the chosen area of the SEM image and A is the selected area.

3 Stretching rate-dependent energy barrier of bubble nucleation

3.1 Models

According to classical nucleation theory, bubble nucleation in polymer foaming is expressed by Eq. (3), comprising the volume energy difference and surface energy difference [8]:

$$\Delta G = -\frac{4\pi}{3}R^3\left(P_{bubble} - P_{sys}\right) + 4\pi R^2\gamma \qquad (3)$$

where P_{bubble} and P_{sys} are the pressures in the bubble nucleus and in the system, respectively. γ is the surface tension between gas and liquid.

However, the classical nucleation theory cannot be fully accepted in the polymer foaming process due to the polymer's viscoelastic nature. Referring to a theory of stretching-induced craze formation of the polymer, Wang et al. [18] introduced elastic strain energy densities, Δg_{eb} and Δg_{st}, into the Gibbs free energy:

$$\Delta G = -\frac{4\pi}{3}R^3\left\{\left(P_{bubble} - P_{sys}\right) - \Delta g_{eb} + \Delta g_{st}\right\} + 4\pi R^2\gamma \qquad (4)$$

$$\Delta g_{st} = \Delta g_h + \Delta g_d \qquad (5)$$

Δg_{eb} denotes the critical distortion energy density, and Δg_{st} is the total elastic strain energy density, which is further divided into the dilatational energy density, Δg_h, and distortional energy density, Δg_d. The continuum mechanism [24-25] and the von Mises theory [26-33] give those energy densities as a function of Poisson's ratio, v, the elastic modulus, E, the dilatational stress, σ_h, von Mises stress, σ_{vm}, the stress at yield, σ_e, yield stress, σ_y and dimensionless constant, μ. The details of those functions are given by Eq. S1 in the Supporting Information.

The homogenous bubble nucleation activation energy barrier for tensile stress was given by:

$$\Delta G_{hom}^{*} = \frac{16\pi\gamma^3}{3\{(P_{bubble}-P_{\mathrm{sys}})+\Delta g_{st}-\Delta g_{eb}\}^2} \quad (6)$$

Considering the presence of the nucleating agent, the heterogenous bubble nucleation activation energy barrier can be expressed as:

$$\Delta G_{het}^{*} = \frac{16\pi\gamma^3}{3\{(P_{bubble}-P_{\mathrm{sys}})+\Delta g_{st}-\Delta g_{eb}\}^2} f(\theta,\beta) \quad (7)$$

where $f(\theta,\beta)$ represents a term related to surface geometry β of nucleating agent and the wetting factor θ.

The homogenous bubble nucleation energy barrier became a function of Δg_{st} and Δg_{eb} in addition to the degree of supersaturation, $P_{bubble} - P_{\mathrm{sys}}$, and surface tension, γ. Based on these Eqs. (4)-(6), Wang et al. qualitatively explained why stretching or compressing the polymers before batch physical foaming could enhance bubble nucleation. However, they did not consider the effect of the stretching rate on the dilatational and distortional energy densities.

In this study, we took into account the strain rate dependency when formulating both energy densities, Δg_{st} and Δg_{eb}, based on the yield criterion that Yu et al. proposed [34]. They developed a strain rate-dependent yield criterion, starting the following constitutive equation of a linear elastic stage of orthotropic materials. Using rectangular Cartesian coordinates with principal stress (σ_1, σ_2, σ_3) and strain (ε_1, ε_2, ε_3), they described the strain rate-dependent yield criterion. When considering the uniaxial loading (stretching or compressing) direction (axis-1), they derived the distortional strain energy density, u_d, and the total strain energy density, u_ϵ, as follows:

$$u_d = A_1\varepsilon_1^2 + A_2\varepsilon_1\dot{\varepsilon}_1^n \quad (8)$$

$$u_\epsilon = \frac{1}{2}B_1\varepsilon_1^2 + \frac{1}{2}B_2\varepsilon_1\dot{\varepsilon}_1^n \quad (9)$$

where A_1, A_2, B_1, and B_2 are defined by

$$A_1 = \frac{1}{2}(k_{11} - v_{21}k_{12} - v_{31}k_{13}) - \frac{1}{18}\sum_{i,j=1}^{3} k_{ij}\,(1 - v_{21} - v_{31})^2$$

$$A_2 = \frac{1}{2}(f_{11} + (-v_{21})^n f_{12} + (-v_{31})^n f_{13}) - \frac{1}{2} \cdot \frac{1}{3^{n+1}} \sum_{i,j=1}^{3} f_{ij} \, (1 - v_{21} - v_{31})^{n+1}$$

$$B_1 = k_{11} - v_{21} k_{12} - v_{31} k_{13}$$

$$B_2 = f_{11} + (-v_{21})^n f_{12} + (-v_{31})^n f_{13}$$

where $\{v_{ij}\}$ are Poisson's ratios. $k_{ij}$are the elastic stiffness coefficients in the constitutive equation, relating between strain and stress by Hooke's law [34, 35]. f_{ij} are the coefficients, expressing the relationship between the stress and strain rate. The constitutive equation is denoted by Eq. (S2-1) in the Supporting Information, and the matrices are shown in Eq. (S2-2).

Then, they gave a yield criterion as a relationship between the critical distortional energy density, u_{ds}, and the distortional energy density, u_d.

$$u_d \leq u_{ds} = \frac{1+v}{3E} \sigma_y^2 \qquad (10)$$

Assuming the critical distortional energy density governs the yield, the relationship among the critical distortional energy density, u_{ds}, yield stress, σ_y, and yield strain, ε_y, was derived using Eqs. (11)-(12) as

$$u_{ds} = A_1 \varepsilon_y^2 + A_2 \varepsilon_y \dot{\varepsilon}_1^n \qquad (11)$$

$$\sigma_y = B_1 \varepsilon_y + B_2 \dot{\varepsilon}_1^n \qquad (12)$$

We used their critical distortional energy density, u_{ds}, (Eq. (11)) as Δg_{eb} and their total strain energy density, u_ϵ (Eq. (9)) as Δg_{st} in the Gibbs free energy of bubble nucleation (Eq. (4)), i.e.,

$$\Delta g_{eb} = A_1 \varepsilon_y^2 + A_2 \varepsilon_y \dot{\varepsilon}_1^n \qquad (13)$$

$$\Delta g_{st} = \frac{1}{2} B_1 \varepsilon_1^2 + \frac{1}{2} B_2 \varepsilon_1 \dot{\varepsilon}_1^n \qquad (14)$$

Substituting Eqs. (13) and (14) into Eq. (6) gives the homogenous nucleation energy barrier under tensile stress in combination with the strain rate:

$$\Delta G_{hom}^* = \frac{16\pi\gamma^3}{3\left[\left(P_{bubble} - P_{\mathrm{sys}}\right) + \frac{1}{2} B_1 \varepsilon_1^2 + \frac{1}{2} B_2 \varepsilon_1 \dot{\varepsilon}_1^n - (A_1 \varepsilon_y^2 + A_2 \varepsilon_y \dot{\varepsilon}_1^n)\right]^2} \qquad (15)$$

The heterogenous bubble nucleation activation energy barrier can be expressed as:

$$\Delta G_{het}^{*} = \frac{16\pi\gamma^3}{3\left[\left(P_{bubble}-P_{\mathrm{sys}}\right)+\frac{1}{2}B_1\varepsilon_1^2+\frac{1}{2}B_2\varepsilon_1\dot{\varepsilon}_1^n-\left(A_1\varepsilon_y^2+A_2\varepsilon_y\dot{\varepsilon}_1^n\right)\right]^2} f(\theta,\beta) \qquad (16)$$

To use Eqs. (15) and (16), A_1, A_2, B_1, B_2 and n must be identified. In this study, Poisson's ratio v_{ij} is assumed to be strain rate-independent [36] and equal in value for all directions, i.e., $v_{ij}= v$ (constant). It was assumed to be 0.49 (SIBS is a type of elastomer whose Poisson's ratio is generally close to 0.5). To determine these parameter values, one-directional stretching tests with various stretching rates were needed.

3.2 Tensile Test for Determining Energy Density Parameters

Tensile tests with various stretching rates were performed, including one quasi-static test (1 mm/min) and four dynamic tests (50, 100, 200, and 400 mm/min). First, a yield point $(\varepsilon_y, \sigma_y)$ was determined from the one quasi-static test result. The critical distortional energy density, u_{ds}, was determined by Eq. (10) with the obtained σ_y and E. Then, A_1 was calculated using Eq. (11) with ε_y, assuming that the stretching rate, $\dot{\varepsilon}_1$, was regarded as zero for the quasi-static test data. Then, A_2 was determined by transforming Eq. (11) into Eq. (17) using other dynamic test data with the calculated A_1 value.

$$\log\left(\frac{u_{ds}}{\varepsilon_y} - A_1\varepsilon_y\right) = \log(A_2) + n\log(\dot{\varepsilon}_1) \qquad (17)$$

Similarly, B_1 was determined by Eq. (12) using ε_y and σ_y of quasi-static test data. Then, B_2 was determined by transforming Eq. (12) into Eq. (18) and using more than four sets of ε_y, σ_y and constant stretching rate, $\dot{\varepsilon}_1$, data.

$$\log(\sigma_y - B_1\varepsilon_y) = \log(B_2) + n\log(\dot{\varepsilon}_1) \qquad (18)$$

Another method of determining A_1 and B_1 values with Poisson's ratio and the elastic modulus, E, which Yu et al. proposed [34], was summarized and performed in the Supporting Information.

4 Results and discussion

4.1 Tensile Test Data and Parameter Values

Figure 1 shows strain–stress curves of quasi-static and dynamic tests of solid samples of SIBS073T and SIBS062M, respectively. These results demonstrated an increase in the yield stress with increasing stretching rate.

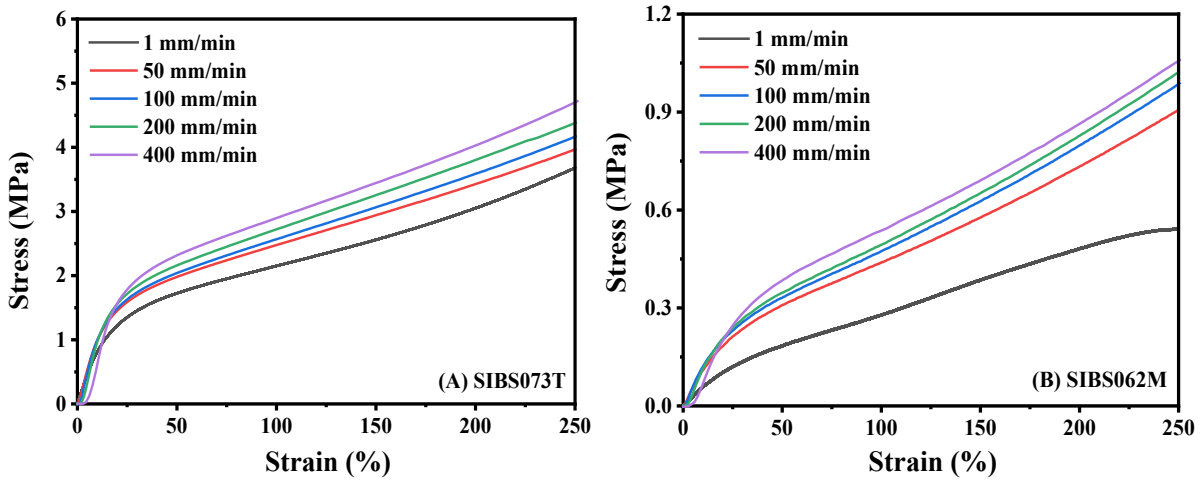

Figure 1. Strain–stress (S–S) curves of quasi-static and dynamic tests of solid samples. (A): SIBS073T and (B): SIBS062M.

Figure 2 shows how to obtain ε_y and σ_y from a S–S curve of the tensile test. The black dashed line was drawn as a slope of the linear part of the strain–stress curve. Then, the dashed line was shifted to a 0.2% strain offset called the 0.2% offset method [37] and intersected with the S–S curve. The crossover point is regarded as the yield point. As a consequence, ε_y and σ_y were obtained. The parameter values of A_1, A_2, B_1, B_2 and n were determined by following the procedure described in the previous section, as listed in Table 2.

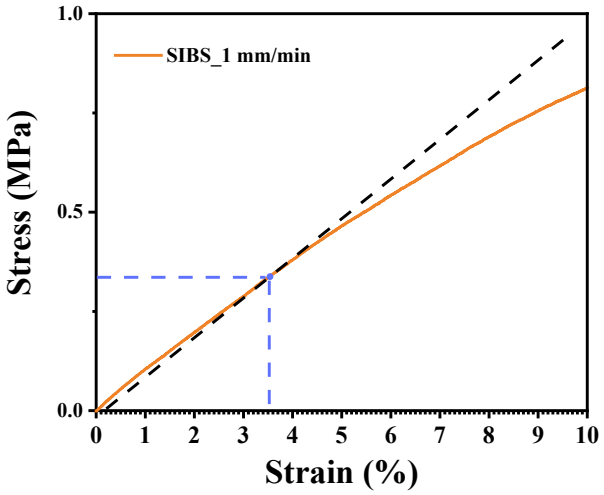

Figure 2. Scheme of determining ε_y and σ_y from S–S curve.

Table 2. Estimated parameter values from quasi-static and dynamic tensile tests of different grades of SIBS.

Parameters	SIBS073T	SIBS062M
A_1 (MPa)	4.76	0.37
A_2 (MPa·s^n)	-4.34×10^{-1}	-6.59×10^{-2}
B_1 (MPa)	9.56	0.74
B_2 (MPa·s^n)	5.50×10^{-1}	1.39×10^{-1}
Δg_{eb} in quasi-static test (MPa)	6.17×10^{-3}	1.70×10^{-4}
n	0.47	0.57
Poisson's ratio	0.49	0.49

4.2 Stretching-induced foaming

Figure 3 shows a series of snapshots of stretching-induced foaming at a 50 mm/min stretching rate with 300% final strain. The gas-laden SIBS samples were prepared by reducing the delivery pressure to 5 MPa to suppress the bubble nucleation caused by supersaturation, $P_{bubble} - P_{\text{sys}}$.

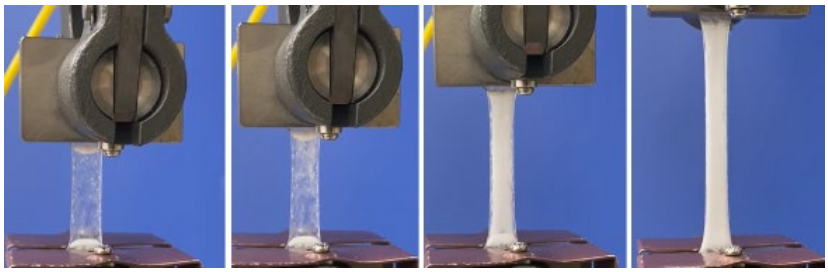

Figure 3. A series of snapshots of stretching-induced foaming at 50 mm/min stretching rate with 300% final strain (gas delivery pressure: 5 MPa).

The sample became white due to the occurrence of bubble nucleation in the polymer, and the whiteness increased as the strain increased. The digital camera images of SIBS samples before and after being stretched to 300% linear strain are given in Figures S1 and S2 in the Supporting Information.

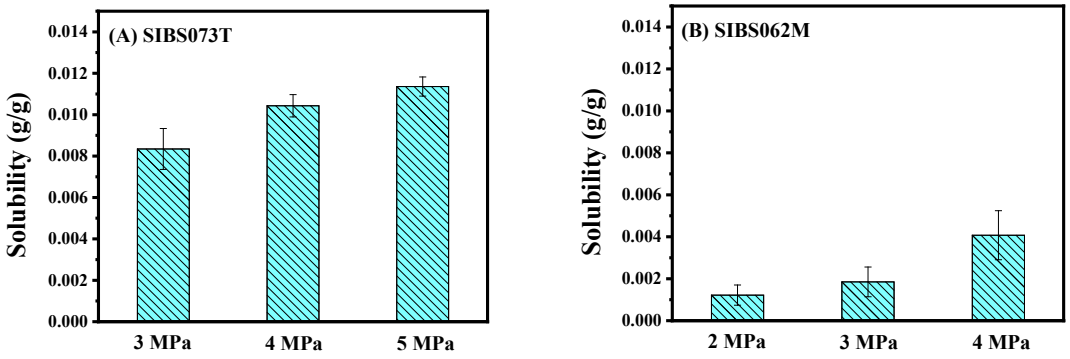

Figure 4. CO_2 contents in SIBS before stretching at room temperature.

To clarify the effects of gas contents, elastic modulus, and stretching rates on cell structure, stretching-induced foaming experiments were carried out by changing the gas delivery pressure of the injection molding process at three levels and the stretching rate of the tensile test for two grades of SIBS (073T and 062M) with different elastic moduli. The maximum strain was set to 300%, and the stretching rate was changed at four levels (50, 100, 200, and 400 mm/min).

Figure 4 shows the gas content of the gas-laden SIBS just after removing the samples from the injection molding process. The contents were calculated from the weight gain of the sample prepared under the designated gas delivery from one with no gas delivery. Because gas diffusion existed during weighing and the foam injection molding machine could not achieve the gas/polymer phase equilibrium, the gas contents were not equivalent to the equilibrium solubility of CO_2 in SIBS. On the other hand, the weight gain reflected the gas contents before stretching. The important point that Figure 4 indicates is that the CO_2 content in SIBS increased with increasing delivery pressure at FIM.

4.3 Effect of pressure on cell structure

Figure 5 shows the effect of CO_2 content on the cell structure of stretching-induced foams of SIBS073T prepared by stretching at the maximum stretching rate of 400 mm/min to 300% strain. When delivering CO_2 to SIBS062M at 5 MPa, it was not easy to prevent foaming caused by supersaturation. While delivering CO_2 to SIBS073T at 2 MPa, no foaming occurred

during the stretching process. In addition, the bubble density increased as the CO_2 content increased for both polymers. SIBS062M foams showed a larger bubble size than SIBS073 because SIBS062M has a lower CO_2 content, as shown in Figure. 4.

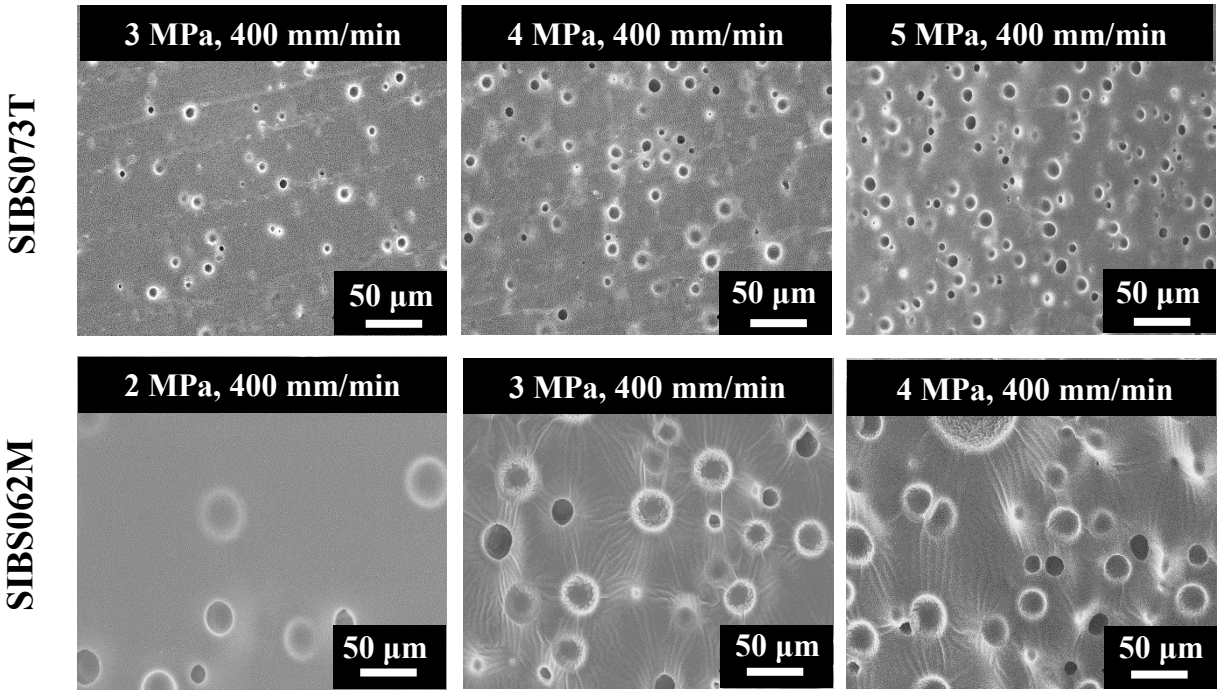

Figure 5. SEM images of the stretching-induced foams of SIBS073T and 062M with various pressures.

4.4 Effect of stretching rate on cell structure

Figure 6 shows the SEM images of the cell structure of the stretching-induced foam of SIBS073T prepared at different stretching rates, 50, 200, and 400 mm/min, with 300% strain under 5 MPa delivery pressure. The SEM images of unstretched-CO_2-laden SIBS073T and SIBS062M, prepared at different delivery pressures, were given in Figures S7 and S8 of Supporting Information, showing a few large bubbles were observed than the stretching-induced foaming samples.

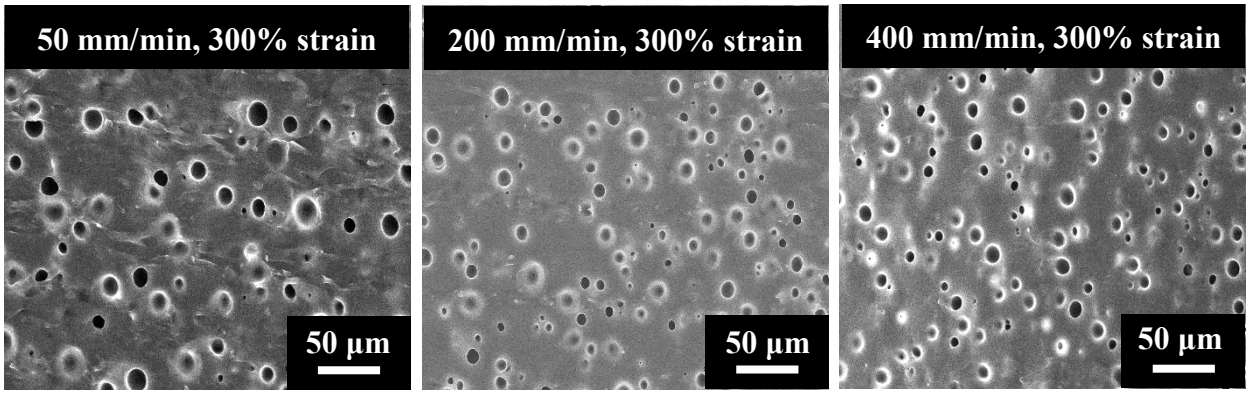

Figure 6. SEM images of the cell structure of stretching-induced foams of SIBS073T at different stretching rates (50, 200 and 400 mm/min) with strains of 300% and 5 MPa delivery pressure.

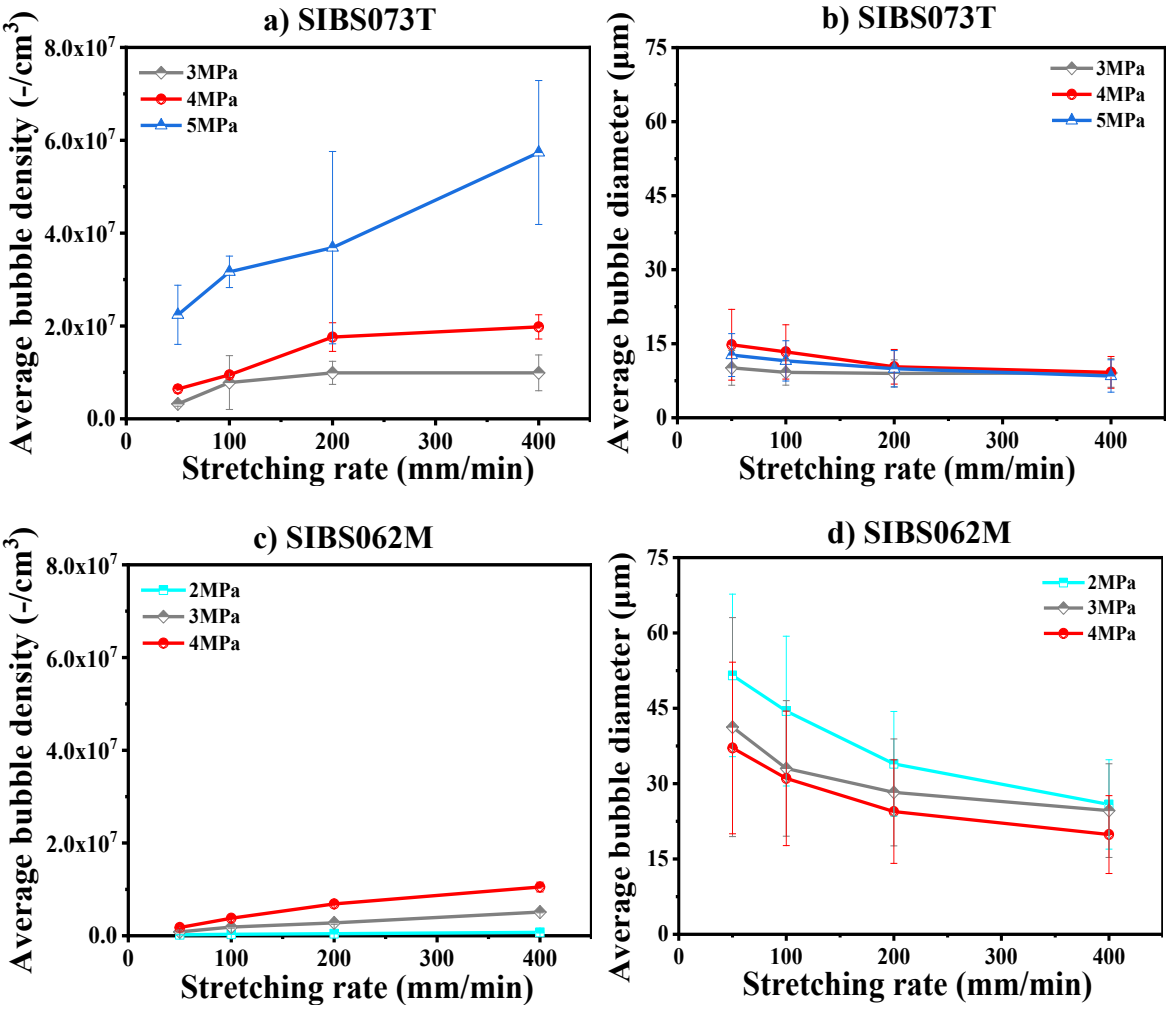

Figure 7. Bubble densities and diameters of stretching-induced SIBS073T (a, b) and SIBS062M (c, d) foams prepared at different stretching rates with 300% strain.

As the stretching rate increased, the bubble density increased, and the bubble size decreased. These trends can be clearly observed in Figure 7. Figure 7 shows the bubble density and diameter of the stretching-induced foams of SIBS073 prepared at different stretching rates with 300% strain.

When the stretching rate and strain were set to 400 mm/min and 300%, respectively, with 5 MPa CO_2 delivery pressure, the bubble density was approximately 5.74×10^7 bubbles/cm^3, which was approximately 2.6 times greater than that prepared at 50 mm/min with 5 MPa CO_2 delivery pressure (Figure 7a). The sensitivity of the bubble density to the stretching rate increased as the CO_2 content increased. When comparing Fig. 7a with 7c, it can be said that the bubble nucleation in the higher elastic SIBS is more sensitive to the stretching rate.

These trends can be explained using Gibbs free energy equation, Eqs. (15) and (16), with the estimated A_2 and B_2 values. Because A_2 is negative and B_2 is positive, with the increased stretching rate, the denominator of Eqs. (15) and (16) increases, and the energy barrier is lower. As a consequence, bubble nucleation is promoted by an increased stretching rate. Comparing these values of SIBS073T with those of SIBS062M, the values of SIBS073 are larger. As a result, the sensitivity of bubble density to the stretching rate becomes greater with SIBS073T than with SIBS062M.

Furthermore, the gas content in the polymer before stretching was increased when the gas delivery pressure was increased. Thus, the degree of supersaturation term in Eqs. (15) and (16), $\left(P_{bubble} - P_{\mathrm{sys}}\right)$, should become more significant as the gas content increases. Since the bubble nucleation rate, J, is an exponential function of $\Delta G^*_{\mathrm{hom}}$, or $\Delta G^*_{\mathrm{het}}$, i.e., $J \propto \exp(-\frac{\Delta G^* hom}{kT})$ or $\exp(-\frac{\Delta G^* het}{kT})$, the sensitivity of bubble nucleation to the stretching rate is greater at higher gas contents.

4.5 Effect of strain on cell structure

Figure 8 summarizes the bubble densities and diameters of the stretching-induced foams of SIBS073T and SIBS062M with different strains. Figures S4 and S5 show the SEM images with various strains. Stretching was performed at a 400 mm/min stretching rate with three different final strains, 100, 200, and 300%, just after removing the polymer from the FIM,

where the gas delivery pressure was changed at three levels. As the strain increased, the bubble density increased, and the bubble size decreased. The sensitivity of the bubble density of SIBS073T to the final strain was greater than that of SIBS062M, and the bubble nucleation barrier difference for SIBS073T and SIBS062M could be a key factor that affected the foam morphology. The sensitivity increased with the gas delivery pressure.

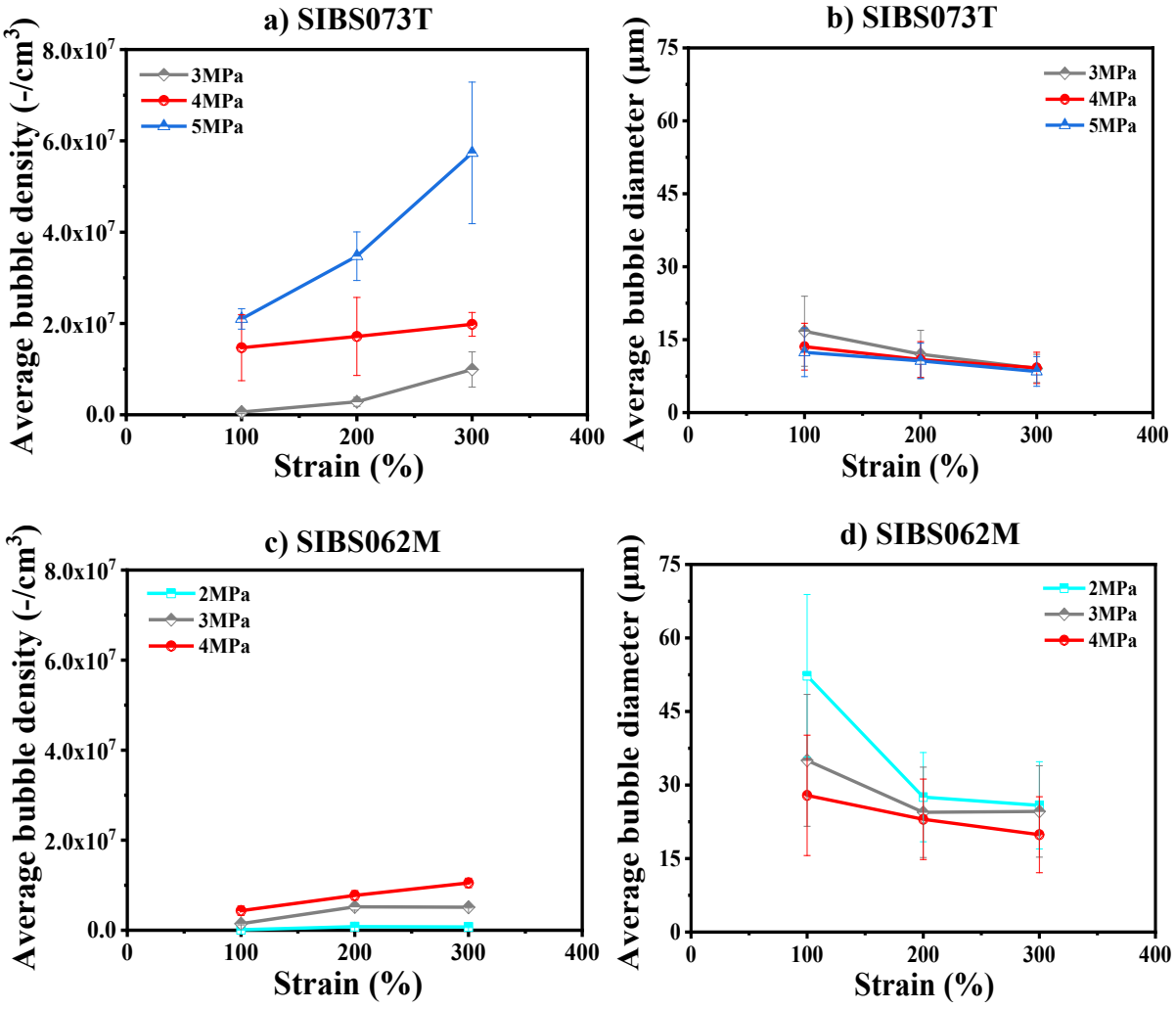

Figure 8. Bubble densities and diameters of stretching-induced foams of SIBS073T (a, b) and SIBS062M (c, d) at three different strains with a 400 mm/min stretching rate.

These experimental results can also be explained using Eq. (14) with the estimated B_1 and B_2 values. Both values are positive, and ΔG_{hom} was decreased by increasing the strain, ε_1. Then, bubble nucleation was enhanced. Comparing the B_1 and B_2 values of SIBS073T with those of SIBS062M, the values of SIBS073 are larger than those of SIBS062M. As a result,

the sensitivity of bubble density to the strain becomes greater with SIBS073T than with SIBS062M. The effect of the gas delivery pressure on the sensitivity can be explained in the same way as the effect of the stretching rate on the bubble nucleation at different gas delivery pressures.

5. Conclusion

In this research, we conducted the stretching-induced foaming of a TPE, SIBS, using a tensile tester and foam injection molding machine. Two grades of SIBS with different elastic moduli were used. We fabricated foams with different bubble densities and sizes by changing the gas content of the gas-laden TPE, stretching rate, and final strain. We found that the larger the gas content was, the more significant the stretching rate and stretching amount (final strain) promoted bubble nucleation, compared with unstretched gas-laden samples. TPU was also used for stretching-induced foaming, which shows similar conclusion with different stretching rates in Supporting Information. Furthermore, the higher the elastic modulus TPE was stretched, the more significant the stretching rate and amount (final strain) promoting bubble nucleation. These experimental results suggested that the distortion energy and the elastic strain energy are essential factors of the thermoplastic elastomer foaming process and effectively enhance bubble nucleation. We could explain these experimental results by employing the Gibbs free energy of the classical nucleation theory for bubble nucleation with critical distortion and the total elastic strain energy density terms described as functions of stretching rate and strain. The increase in the stretching rate and stretching amount reduces the energy barrier of bubble nucleation and provides an extra driving force of bubble nucleation.

The proposed bubble nucleation rate model is not precise enough to simulate the cell morphology, i.e., bubble density and size of the stretching-induced foaming. When CO_2-laden elastomers are prepared, the plasticization effect may occur and change the rheological property, which affects the value of parameters A_1, A_2, B_1, and B_2 of the proposed model because these parameter values are determined from the rheological property. To precisely simulate the cell morphology of stretching-induced foaming, the plasticization effect on the elastic modulus, surface tension, and viscosity should be considered with the combination of the nucleation model with a bubble growth and total mass balance models.

The knowledge obtained through this study can be utilized for practical foam processing of TPE, where it has been considered that TPE's physical foaming is difficult to perform. One directional or biaxial stretching just after foam extrusion dies would enhance bubble nucleation and produce microcellular TPE by a physical foaming agent.

References

[1] G. Wu, P. Xie, H. Yang, K. Dang, Y. Xu, M. Sain, L. S. Turng, W. Yang, A review of thermoplastic polymer foams for functional applications, *J. Mater. Sci.* 56 (2021) 11579–11604. https://doi.org/10.1007/s10853-021-06034-6.

[2] M. Shimbo, I. Higashitani, Y. Miyano, Mechanism of strength improvement of foamed plastics having fine bubble, *J. Cell. Plast.* 43 (2007) 157–167. https://doi.org/10.1177/0021955X06075585.

[3] A. Huang, X. F. Peng, L. S. Turng, In-situ fibrillated polytetrafluoroethylene (PTFE) in thermoplastic polyurethane (TPU) via melt blending: effect on rheological behavior, mechanical properties, and microcellular foamability. *Polymer* 134 (2018) 263–274. https://doi.org/10.1016/j.polymer.2017.11.053.

[4] G. Wang, J. Zhao, G. Wang, L. H. Mark, C. B. Park, G. Zhao, Low-density and structure-tunable microcellular PMMA foams with improved thermal-insulation and compressive mechanical properties, *Eur. Polym. J.* 95 (2017) 382–393. https://doi.org/10.1016/j.eurpolymj.2017.08.025.

[5] G. Wang, G. Zhao, G. Dong, Y. Mu, C. B. Park, G. Wang, Lightweight, super-elastic, and thermal-sound insulation bio-based PEBA foams fabricated by high-pressure foam injection molding with mold-opening. *Eur. Polym. J.* 103 (2018) 68–79. https://doi.org/10.1016/j.eurpolymj.2018.04.002.

[6] E. Gourdon, M. Seppi, On the use of porous inclusions to improve the acoustical response of porous materials Analytical model and experimental verification, *Appl. Acoust.* 71 (2010) 283–298. https://doi.org/10.1016/j.apacoust.2009.11.004.

[7] G. Fontaras, N. Zacharof, B. Ciuffo, Fuel consumption and CO_2 emissions from passenger cars in Europe – Laboratory versus real-world emissions, *Prog. Energy Combust. Sci.* 60 (2017) 97–131. https://doi.org/10.1016/j.pecs.2016.12.004.

[8] J. S. Colton, J. Suh, The nucleation of microcellular thermoplastic foam with additives: part I:

theoretical considerations, *Polym. Eng. Sci.* 27 (1987) 485–492. https://doi.org/10.1002/pen.760270702.

[9] J. H. Han, C. D. Han, A study of bubble nucleation in a mixture of molten polymer and volatile liquid in a shear flow field, *Polym. Eng. Sci.* 28 (1988) 1616–1627. https://doi.org/10.1002/pen.760282408.

[10] S. T. Lee, Shear effects on thermoplastic foam nucleation, *Polym. Eng. Sci. 33* (1993) 418–422. https://doi.org/10.1002/pen.760330707.

[11] S. T. Lee, More experiment on thermoplastic foam nucleation. *J. Cell. Plast.* 30 (1994) 444–453. https://doi.org/10.1177/0021955X9403000502.

[12] L. Chen, X. Wang, R. Straff, K. Blizard, Shear stress nucleation in microcellular foaming process. *Polym. Eng. Sci.* 42 (2002) 1151–1158. https://doi.org/10.1002/pen.11019.

[13] M. C. Guo, Y. C. Peng, Study of shear nucleation theory in continuous microcellular foam extrusion, *Polym. Test.* 22 (2003) 705–709. https://doi.org/10.1016/S0142-9418(03)00004-7.

[14] A. S. Wong, R. Chu, S. N. Leung, C. B. Park, J. H. Zong, A batch foaming visualization system with extensional stress-inducing ability. *Chem. Eng. Sci*. 66 (2011) 55–63. https://doi.org/10.1016/j.ces.2010.09.038.

[15] A. Wong, C. B. Park, The effects of extensional stresses on the foamability of polystyrene-talc composites blown with carbon dioxide, *Chem. Eng. Sci.* 75 (2012) 49–62. https://doi.org/10.1016/j.ces.2012.02.040.

[16] A. Wong, C. B. Park, A visualization system for observing plastic foaming processes under shear stress, *Polym. Test.* 31 (2012), 417–424. https://doi.org/10.1016/j.polymertesting.2011.12.012.

[17] A. Wong, Y. Guo, C. B. Park, Fundamental mechanisms of cell nucleation in polypropylene foaming with supercritical carbon dioxide—Effects of extensional stresses and crystals, *J. Supercrit. Fluids* 79 (2013) 142–151. https://doi.org/10.1016/j.supflu.2013.02.013.

[18] G. Wang, J. Zhao, K, Yu, L. H. Mark, G. Wang, P. Gong, C. B. Park, G. Zhao, Role of elastic strain energy in cell nucleation of polymer foaming and its application for fabricating

sub-microcellular TPU microfilms, *Polymer* 119 (2017) 28–39. https://doi.org/10.1016/j.polymer.2017.05.016.

[19] P. Gong, T. Taniguchi, M. Ohshima, Nanoporous structure of the cell walls of polycarbonate foams, J. Mater. Sci. 49 (2014) 2605–2617.

[20] L. Wang Y. Hikima, M. Ohshima, A. Yusa, S. Yamamoto, H. Goto, Development of a Simplified Foam Injection Molding Technique and Its Application to the Production of High Void Fraction Polypropylene Foams, *Ind. Eng. Chem. Res.* 56 (2017) 13734–13742. https://doi.org/10.1021/acs.iecr.7b03382.

[21] L. Wang, Y. Wakatsuki, Y. Hikima, M. Ohshima, A. Yusa, H. Uezono, A. Naitou, Preparation of microcellular injection-molded Foams using different types of low-pressure gases via a new foam injection molding technology, *Ind. Eng. Chem. Res.* 58 (2019) 17824−17832. https://doi.org/10.1021/acs.iecr.9b03330.

[22] H. J. Kong, S. H. Lee, D. G. Kim, H. J. Kim, G. W. Park, K. Hyun, Investigation of Thermoplastic Elastomer (TPE) Foaming Process Using Blowing Agent by Rheological and Morphological Methods. *J. Appl. Polym. Sci*. 2019, 136, 47358. https://doi.org/10.1002/app.47358.

[23] V. Kumar, N. P. Suh, A process for making microcellular thermoplastic parts, *Polym. Eng. Sci.* 30 (1990) 1323−1329. https://doi.org/10.1002/pen.760302010.

[24] N. H. Kim, B. V. Sankar, and A. V. Kumar, *Introduction to Finite Element Analysis and Design, 2nd Edition*, John Wiley &Sons Ltd.: New Jersey, 2018.

[25] F. Irgens. Continuum mechanics. Springer: Berlin, 2008.

[26] J. Rottler, M.O. Robbins, Yield conditions for deformation of amorphous polymer glasses, *Phys. Rev. E.* 64 (2001) 051801-1−051801-8. https://doi.org/10.1103/PhysRevE.64.051801.

[27] I. M. Ward, Review: The yield behaviour of polymers, *J. Mater. Sci*. 6 (1971) 1397–1417. https://doi.org/10.1007/BF00549685.

[28] A. Lazzeri, C. B. Bucknall, Applications of a dilatational yielding model to rubber-toughened polymers, *Polymer* 36 (1995), 2895–2902. https://doi.org/10.1016/0032-3861(95)94338-T.

[29] W. Whitney and R. D. Andrews, Yielding of Glassy Polymers: Volume Effects, *J. Polym. Sci., Part C: Polym. Symp*. 16 (1967) 2981–2990. https://doi.org/10.1002/polc.5070160552.

[30] P. B. Bowden, J. A. Jukes, The plastic flow of isotropic polymers, *J. Mater. Sci*. 6 (1972) 52–63. https://doi.org/10.1007/BF00549550.

[31] W. M. H. Verbeeten, M. Sánchez-Soto, M. L. Maspoch, Hydrostatic pressure dependence in tensile and compressive behavior of an acrylonitrile–butadiene–styrene copolymer, *J. Appl. Polym*. *Sci.* 139 (2022) 52295. https://doi.org/10.1002/app.52295.

[32] C. B. Bucknall, New criterion for craze initiation, *Polymer* 48 (2007) 1030–1041. https://doi.org/10.1016/j.polymer.2006.12.033.

[33] R. A. Duckett, S. Rabinowitz, I. M. Ward, The strain-rate, temperature and pressure dependence of yield of isotropic poly(methylmethacrylate) and poly(ethylene terephthalate), *J. Mater. Sci*. 5 (1970) 909–915. https://doi.org/10.1007/BF00574864.

[34] J. Yu, Q. Fei, P. Zhang, Y. Li, D. Zhang, F. Guo, An innovative yield criterion considering stretching rates based on von Mises stress, *J. Press. Vessel Technol.* 142 (2020) 014501-1–014501-6. https://doi.org/10.1115/1.4044908.

[35] X. Du, Q. Zhang, Z. Wan, A nonlinear constitutive model for rayon-rubber composite in the medium stretching rate range, *J. Elastomers Plast.* 27 (1995) 91–99. https://doi.org/10.1177/009524439502700107.

[36] O. I. Okoli, G. F. Smith, The effect of stretching rate and fibre content on the Poisson's ratio of glass/epoxy composites, *Compos. Struct.* 48 (2000) 157–161. https://doi.org/10.1016/S0263-8223(99)00089-6.

[37] C. Henry, K. Rupel, C. Park, J. Costanzo, C. Kaczowka, K. Malik, S. Ghose, Evaluation of an alternate method for determining yield strength offset values for selective laser sintered polymeric materials, *SAMPE 2019 Charlotte, NC* (2019) 20200002670.

Supporting Information

Stretching-induced Foaming of Gas-Laden Thermoplastic Elastomers

Weiyuan Lin, Masahiro Ohshima

Department of Chemical Engineering, Kyoto University, Kyoto 615-8510, Japan

S1. Molecular weight and ratios of hard and soft segments for SIBS073T and 062M

The molecular weights of both grades of SIBSs were measured by gel permeation chromatography (GPC) (Prominence Series, Shimazu, Japan). 5 mL of chloroform was used to dissolve 0.025 g of SIBS. Prior to the SIBS measurement, the molecular weights of two standard solutions (ST1 and ST2) were measured to ensure data validity. ST1 and ST2 are two types of polystyrene solution with different molecular weights. Data analysis was conducted by software of the high-performance liquid chromatography (LC Solution, Shimazu, Japan). The number average molecular weight, $\bar{M}_n$, and the weight average molecular weight, $\bar{M}_W$, of SIBS are listed in Table S1. The ratio of styrene to isobutylene contents is referred to in the paper [1] and given in Table S1.

Table S1. Molecular weights and compositions of both grades of SIBS.

Grade of SIBS	$\bar{M}_n$	$\bar{M}_W$	**Styrene content (%) [1]**	**Isobutylene content (%) [1]**
SIBS073T	58098	81380	30	70
SIBS062M	38909	64603	23	77

S2. Our previous nucleation model in combination of a crazing Theory

We introduced a crazing theory to the bubble nucleation rate equation for describing the foaming of polycarbonate in 2013 [2]. In our paper, elastic modulus was introduced to the Gibbs free energy of bubble or microvoid nucleation:

$$\Delta G_{bubble} = 4\pi {R_b}^2 \gamma + \Delta G_{strain} - \frac{4\pi {R_b}^3}{3}\left(P_{bub} - P_{sys}\right) \quad \text{(S2-1)}$$

$$\Delta G_{strain} = E_{elastic} \int_{\xi}^{\infty} 6R_b^2 \xi^4 \frac{1}{r^6} 4\pi r^2 dr = 8\pi E_{elastic} R_b^2 \xi \quad \text{(S2-2)}$$

where ΔG_{strain} represents strain energy, and $E_{elastic}$ is the shear elastic modulus. R_b is the bubble radius, γ is surface tension, P_{bubble} is the pressure in bubble, and P_{sys} is the pressure of the polymer matrix. ξ is the initial radius of the microvoid or bubble embryo which is regarded to be the radius of the polymer's free volume.

We derived these equations based on the assumption that the strain energy should be needed for a bubble to grow from the initial size of the bubble embryo, ξ to R_b. We still believe that the concept grasped a feature of polymer foaming and can be applied to nanocellular foaming and engineering plastic foaming, where the elastic modulus is high. However, some ambiguities have remained in the equations. One is the definition of ξ. Another is that the equations could not deal with external forces, such as stretching or compressing forces given by environment. We thought our ΔG_{strain} was not versatile enough to take care of the distortion or deformation (shear/strain) rates externally caused.

If we combine our previous knowledge to the bubble nucleation rate equation proposed in this study, the equation will be written by:

$$J = A\ exp\left(-\frac{\Delta G^*_{hom}}{kT}\right) = A\ exp\left(-\frac{16\pi(\gamma + 2E_{elastic}\xi)^3}{3kT\left[(P_{bubble} - P_{\text{sys}}) + \frac{1}{2}B_1\varepsilon_1^2 + \frac{1}{2}B_2\varepsilon_1\dot{\varepsilon}_1^n - (A_1\varepsilon_y^2 + A_2\varepsilon_y\dot{\varepsilon}_1^n)\right]^2}\right)$$

Our previous knowledge makes the numerator be a function of elastic modulus, $16\pi(\gamma + 2E_{elastic}\xi)^3$: The equation indicates that when the shear elastic modulus, $E_{elastic}$, is high, the bubble nucleation rate is reduced and slowed. But, by giving the stretching force externally, the value of denominator becomes large and the bubble nucleation is enhanced.

S3. Some more details of Gibbs free energy that Prof Park's group proposed

Wang et al. [3] introduced an elastic strain energy barrier, ΔG_{eb}, and ΔG_{st}, and their densities into the Gibbs free energy:

$$\Delta G = -\frac{4\pi}{3}R^3\left(P_{bubble} - P_{sys}\right) + 4\pi R^2\gamma + \Delta G_{eb} + \Delta G_{st}$$

$$\Delta G_{eb} + \Delta G_{st} = \Delta G_{eb} + \Delta G_h + \Delta G_d = -\frac{4\pi R^3}{3}(-\Delta g_{eb} + \Delta g_h + \Delta g_d) \quad \text{(S3-1)}$$

$$\Delta g_h = \frac{3}{2}\frac{(1-2v)}{E}\sigma_{\text{h}}^2 \quad \text{(S3-2)}$$

$$\Delta g_d = \frac{1+v}{3E}\sigma_{\text{vm}}^2 \quad \text{(S3-3)}$$

$$\Delta g_{eb} = \frac{1+v}{3E}\sigma_e^2 = \frac{1+v}{3E}(\sigma_y - \mu\sigma_h)^2 \quad \text{(S3-4)}$$

In their notation, ΔG_{st} represents the elastic strain energy stored at the nucleation sites right before bubble nucleation. It is further divided into dilatational energy, ΔG_h, and distortional energy ,ΔG_d. Introducing the energy density (energies per unit volume) $\Delta g_{eb}, \Delta g_h,$ and Δg_d, Gibbs free energy is described with the dilatational and distortional

energies when a bubble with radius R is born. The continuum mechanism [4] and the von Mises theory [5] give Eq. (S3-1) with Poison's ratio, v, and the elastic modulus, E, the dilatational stress, σ_h, von Mises stress, σ_{vm}, the stress at yield, σ_e, yield stress, σ_y and dimensionless constant, μ.

S4. Constitutive equations with elastic stiffness coefficients

Yu et al. [6] developed a yield criterion as a function of strain rate, starting from the following constitutive equation [6-7]:

$$\boldsymbol{\sigma} = \boldsymbol{C\varepsilon} + \boldsymbol{F\dot{\varepsilon}}^n \qquad \text{(S4-1)}$$

where $\boldsymbol{\varepsilon}$ and $\dot{\boldsymbol{\varepsilon}}$ are total strain and strain rate tensors. n is a material constant describing the strain rate sensitivity of stress. C is elastic stiffness matrix relating between strain and stress by Hooke's law. F is the coefficient matrix concerning the stress and strain rate relationship, which is assumed to have similar structure in form with elastic stiffness matrix C. These two matrices are expressed by:

$$C = \begin{bmatrix} k_{11} & k_{12} & k_{13} & & & \\ k_{21} & k_{22} & k_{23} & & & \\ k_{31} & k_{32} & k_{33} & & & \\ & & & k_{44} & & \\ & & & & k_{55} & \\ & & & & & k_{66} \end{bmatrix}, \; F = \begin{bmatrix} f_{11} & f_{12} & f_{13} & & & \\ f_{21} & f_{22} & f_{23} & & & \\ f_{31} & f_{32} & f_{33} & & & \\ & & & f_{44} & & \\ & & & & f_{55} & \\ & & & & & f_{66} \end{bmatrix} \qquad \text{(S4-2)}$$

S5. How to calculate A_1 and B_1 from the elastic stiffness matrix and Poisson's ratio

From the literature [8], we can know the elastic stiffness matrix of an isotropic material (Eq. (S5-1)). If we regard SIBS as an isotropic material, A_1 can be calculated with k_{11}, k_{12} and k_{13} (seen in Eq. (S5-2)).

$$\begin{bmatrix}\sigma_{11}\\ \sigma_{22}\\ \sigma_{33}\\ \sigma_{23}\\ \sigma_{13}\\ \sigma_{12}\end{bmatrix} = \frac{E}{(1+\nu)(1-2\nu)}\begin{bmatrix} 1-\nu & \nu & \nu & 0 & 0 & 0\\ \nu & 1-\nu & \nu & 0 & 0 & 0\\ \nu & \nu & 1-\nu & 0 & 0 & 0\\ 0 & 0 & 0 & \frac{(1-2\nu)}{2} & 0 & 0\\ 0 & 0 & 0 & 0 & \frac{(1-2\nu)}{2} & 0\\ 0 & 0 & 0 & 0 & 0 & \frac{(1-2\nu)}{2}\end{bmatrix}\begin{bmatrix}\varepsilon_{11}\\ \varepsilon_{22}\\ \varepsilon_{33}\\ 2\varepsilon_{23}\\ 2\varepsilon_{13}\\ 2\varepsilon_{12}\end{bmatrix} - \frac{E\alpha\Delta T}{1-2\nu}\begin{bmatrix}1\\1\\1\\0\\0\\0\end{bmatrix} \quad \text{(S5-1)}$$

Using Eqs. (S4-2) and (S5-1) to get k_{ij} (i = 1,2,3, j = 1,2,3) (Poisson's ratio is assumed to be 0.49 and E can be obtained from S-S curve). Then A_1 and B_1 can be obtained by using Eq. (S5-3) and Eq. (S5-4) respectively.

$$\begin{cases} k_{11} = \frac{E}{(1+v)(1-2v)} \times (1-v) \\ k_{12} = \frac{E}{(1+v)(1-2v)} \times (1-v) \\ k_{13} = \frac{E}{(1+v)(1-2v)} \times v \end{cases} \quad \text{(S5-2)}$$

$$A_1 = \frac{1}{2}(k_{11} - v_{21}k_{12} - v_{31}k_{13}) - \frac{1}{18}\sum_{i,j=1}^{3} k_{ij}\,(1 - v_{21} - v_{31})^2$$

(S5-3)

$$B_1 = k_{11} - v_{21}k_{12} - v_{31}k_{13} \quad \text{(S5-4)}$$

where Poisson's ratio v is equal in value for all directions. i.e., $v_{ij} = v$ (constant).

S6. Digital camera image of the stretching-induced foaming.

Figures S1 and S2 show the digital camera picture of unstretched and stretched gas-laden SIBS073T (3, 4, 5 MPa) and SIBS062M (2, 3, 4 MPa) after a few hours after injection molding. The first samples on the left were unstretched. The pictures of stretched samples were taken after stretched to linear strain of 300%. The numbers indicate the stretching rate (1, 2, 3 and 4 represent 50, 100, 200 and 400 mm/min respectively). Stretched samples of all conditions turned white due to foaming, which could be seen in all these pictures.

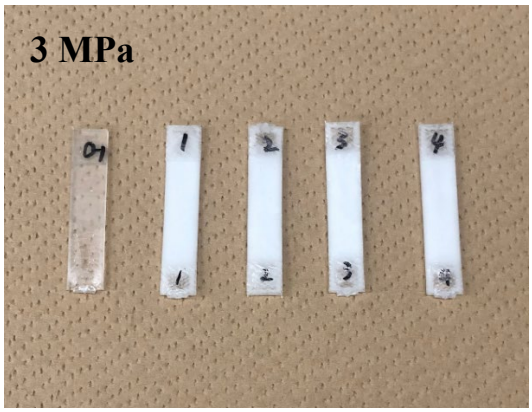

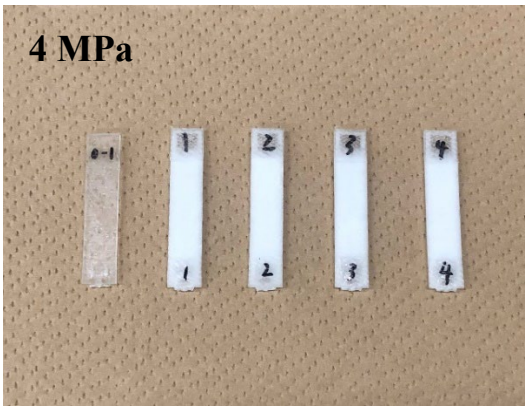

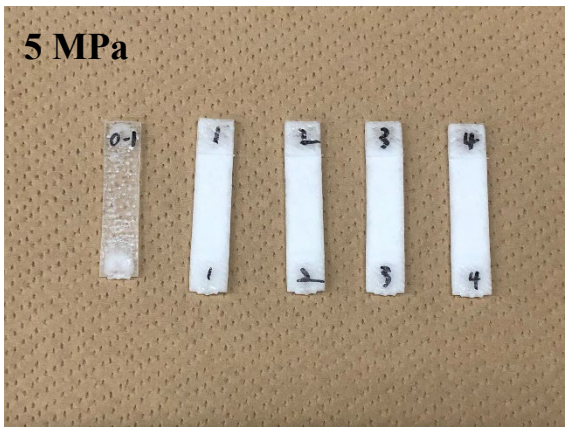

Figure S1. Digital camera picture of unstretched and stretched gas-laden SIBS073T with various pressures.

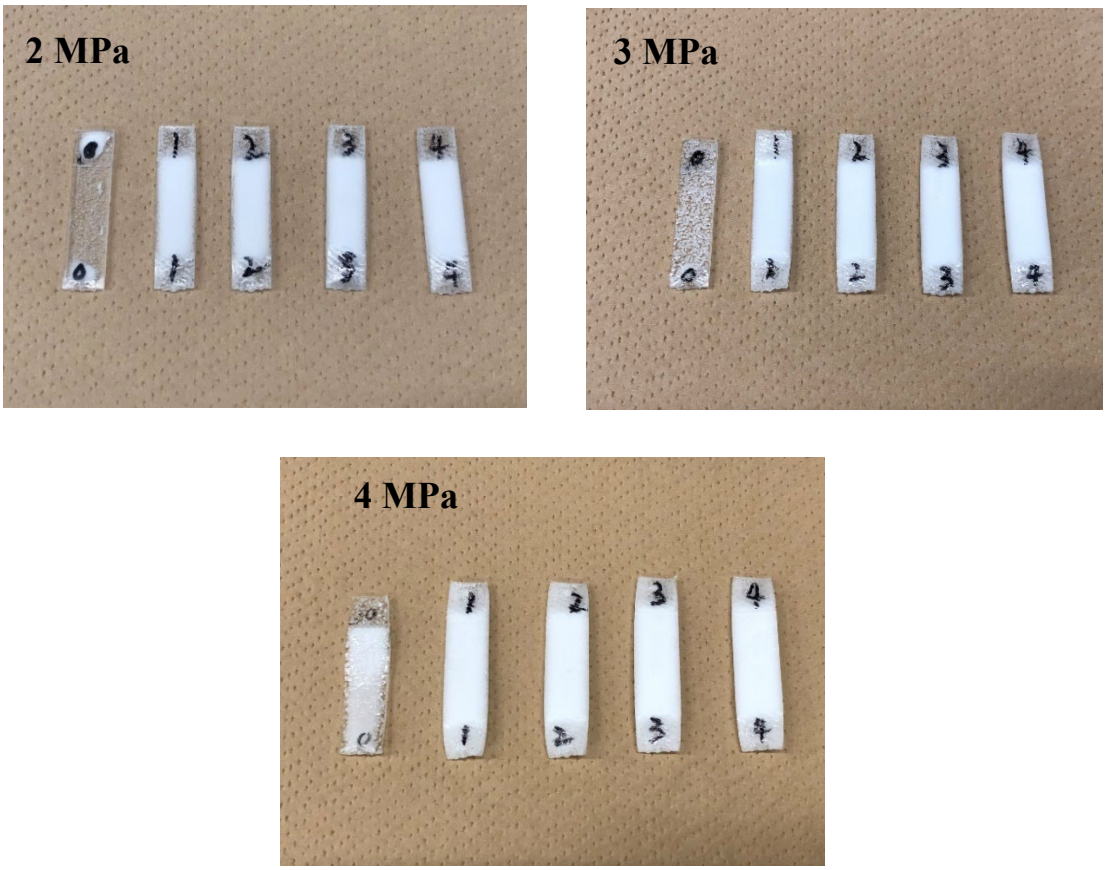

Figure S2. Digital camera picture of unstretched and stretched gas-laden SIBS062M with various pressures.

S7. SEM images of SIBS062M at various stretching rates with 300% stain and 5 MPa delivery pressure

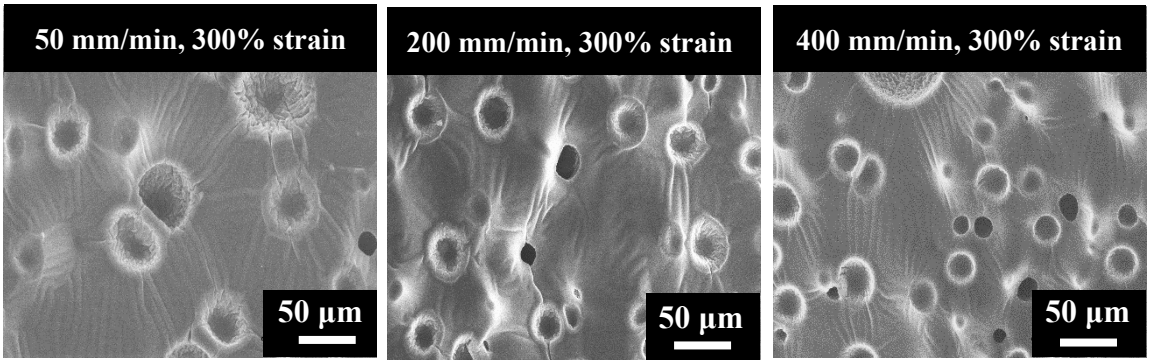

Figure S3. SEM images of cell structure of the stretching-induced foams of SIBS062M at different stretching rates (50, 200 and 400 mm/min) with strain of 300% and 5 MPa delivery pressure.

S8. SEM images of the SIBS073T and 062M stretching-induced foam at various strains with stretching rate of 400 mm/min

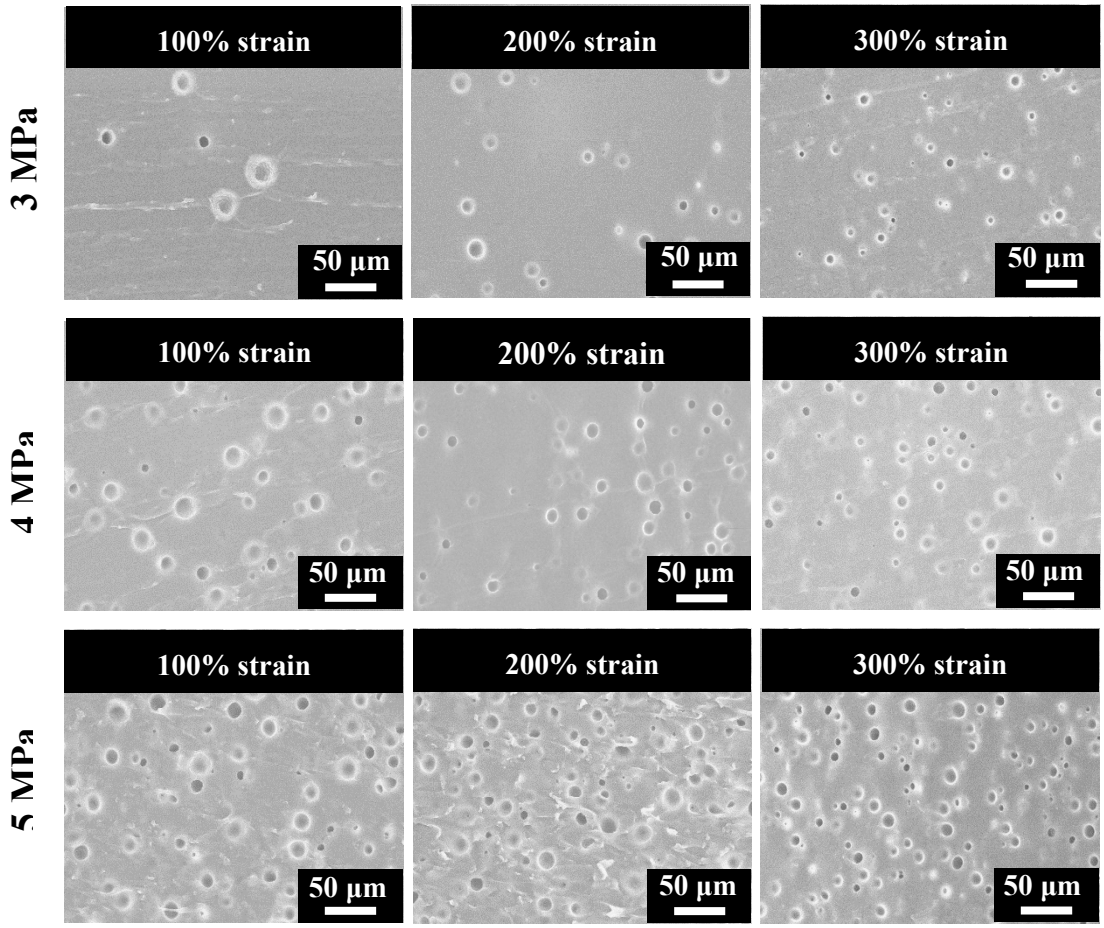

Figure S4. SEM images of cell structure of the stretching-induced foams of SIBS073T at different strains (100, 200 and 300%) with stretching rate of 400 mm/min and 5 MPa delivery pressure.

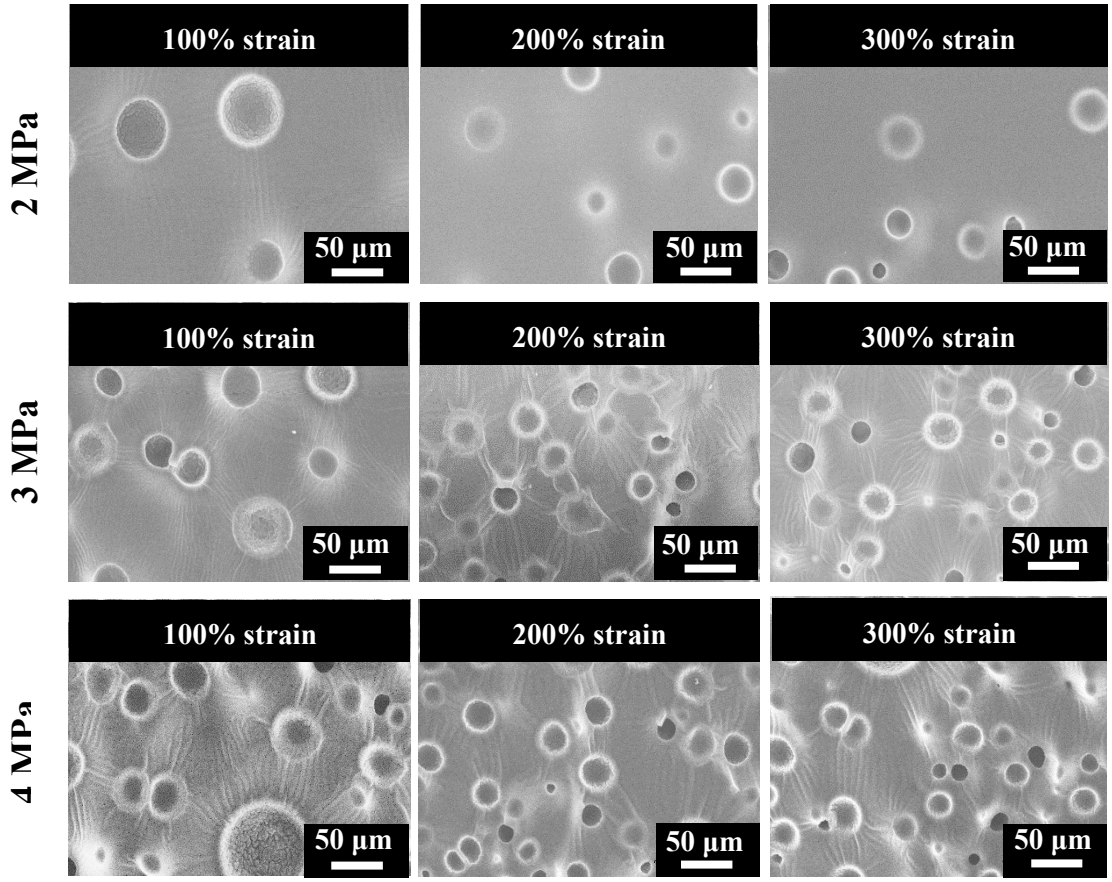

Figure S5. SEM images of cell structure of stretching-induced foams of SIBS062M at different strains (100, 200 and 300%) with stretching rate of 400 mm/min and 5 MPa delivery pressure.

S9. Strain-Stress (S-S) curves of SIBS073T solid samples and nonfoamed CO_2-laden SIBS073T samples (2 MPa)

Figure S6 illustrates the S-S curves of solid SIBS073T and CO_2-Laden SIBS073T Samples (2 MPa). It can be seen that SIBS073T was softened with CO_2, indicating the plasticizing effect of CO_2.

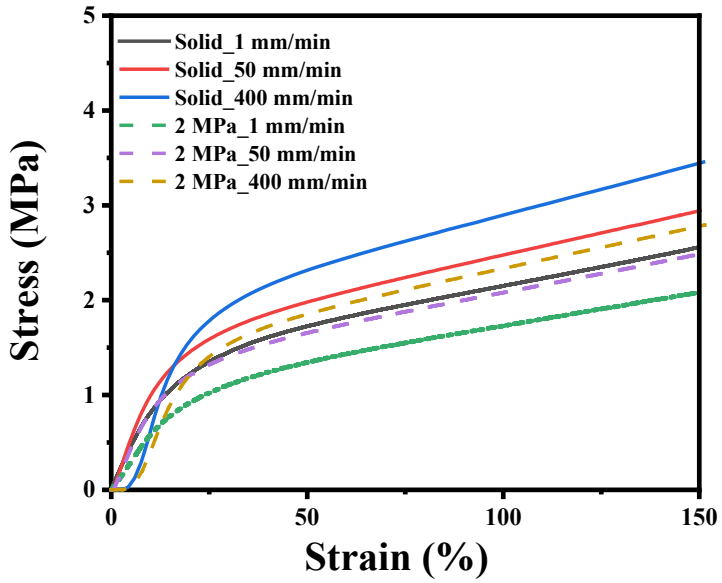

Figure S6. S-S curves of solid SIBS073T and CO_2-laden SIBS073T samples (2 MPa).

Table S2. Comparison of parameter values estimated from quasi-static and dynamic tensile tests of SIBS073T solid and nonfoamed SIBS073T with 2 MPa CO_2.

Parameters	**SIBS073T (solid)**	**SIBS073T (2 MPa)**
A_1 (MPa)	4.76	3.27
A_2 (MPa·s^n)	-4.34×10^{-1}	-1.97×10^{-1}
B_1 (MPa)	9.56	6.30
B_2 (MPa·s^n)	5.50×10^{-1}	4.03×10^{-1}
Δg_{eb} in quasi-static test (MPa)	6.17×10^{-3}	7.47×10^{-3}
n	0.47	0.22
Yield strain in quasi-static test (%)	3.60	4.78
Poisson's ratio	0.49	0.49

S10. SEM images of unstretched CO_2-laden SIBS073T and 062M

Figures S7 and S8 show the SEM images of unstretched-CO_2-laden SIBS073T and 062M prepared at different CO_2 delivery pressures. No bubble was observed in SIBS073T, and a few large bubbles were in SIBS062M. Even though bubbles were observed in unstretched SIBS062, the bubble density was lower and the bubble size was larger than those of the stretched samples. Comparison of bubble density and size before and after stretching indicates that the stretching enhances the bubble nucleation.

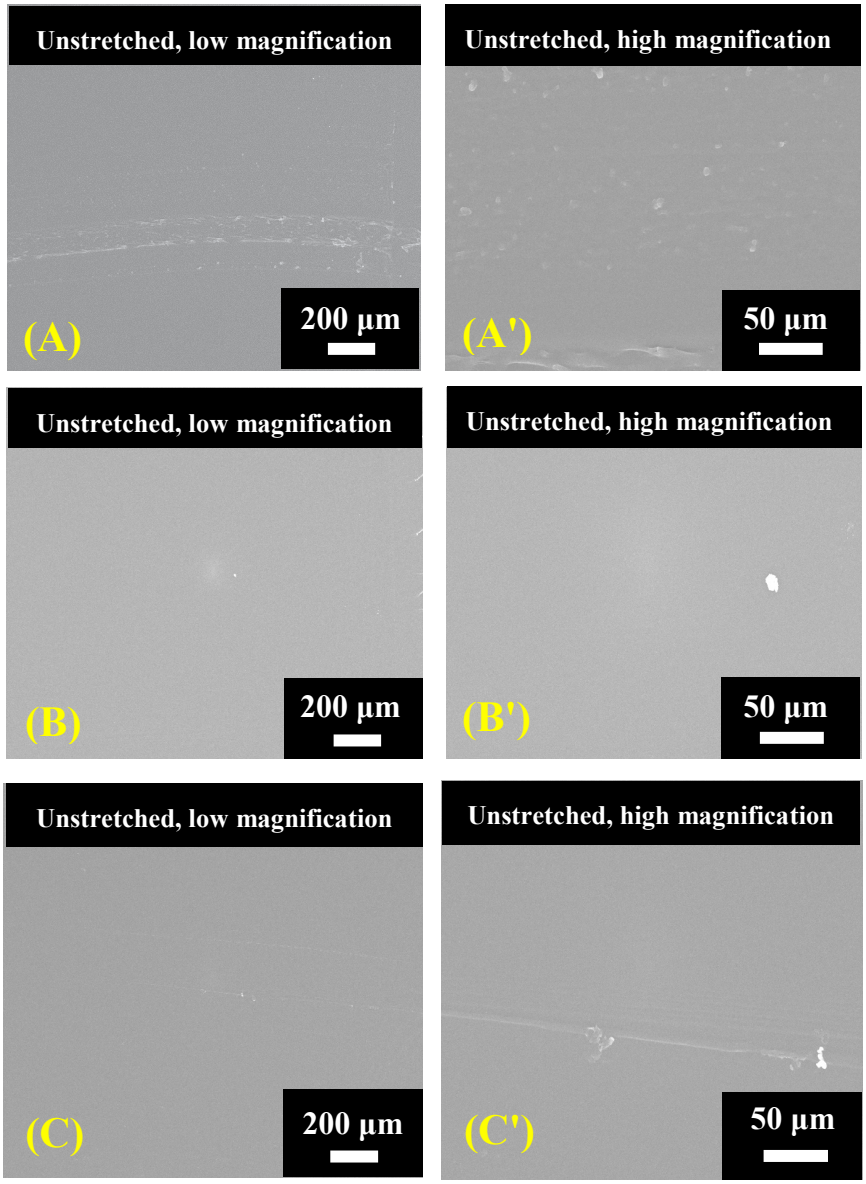

Figure S7 SEM images of unstretched CO_2-laden SIBS073T samples with different CO_2 delivery pressures: (A)-(C) are low magnification images and (A')-(C') are high magnification ones: ((A) and (A'): 3MPa, (B) and (B'): 4MPa, (C) and (C'): 5MPa).

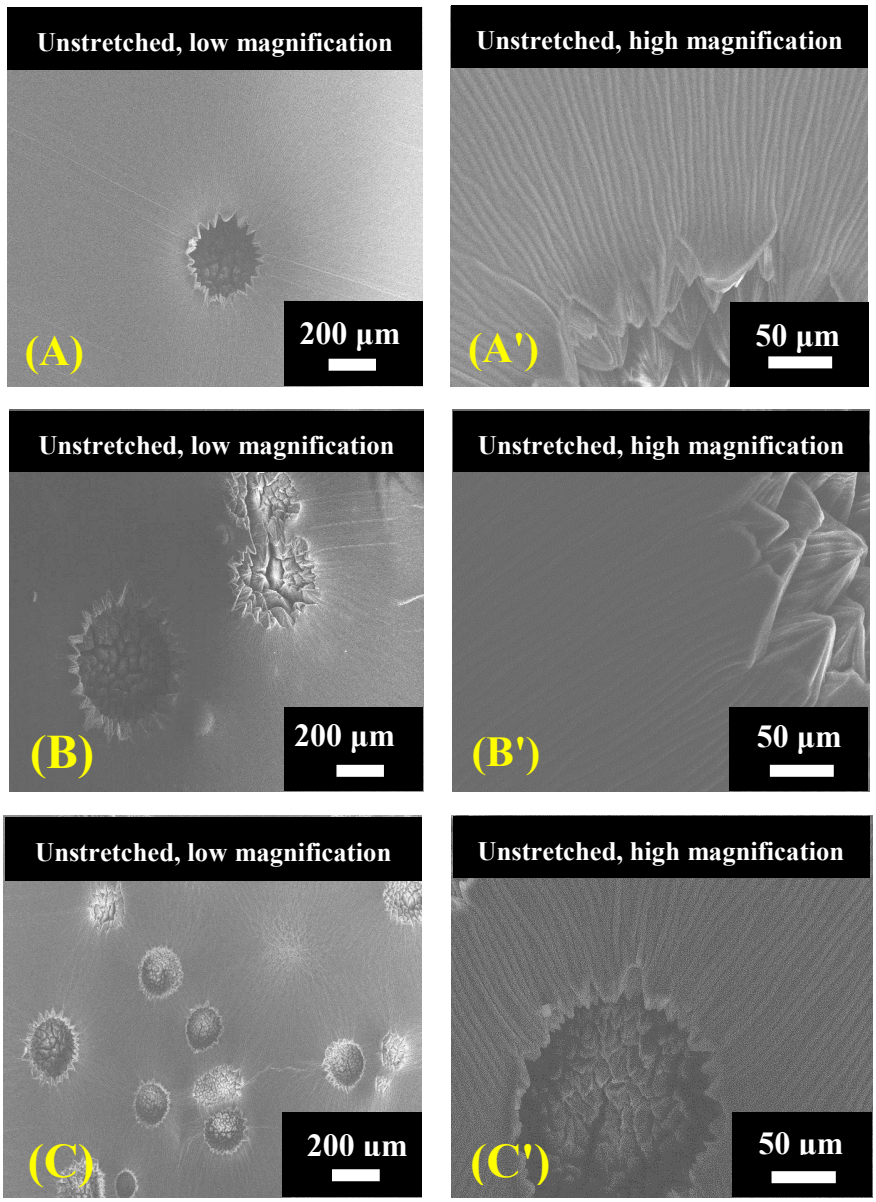

Figure S8 SEM images of unstretched CO_2-laden SIBS062M samples with different CO_2 delivery pressures: (A)-(C) are low magnification images and (A')-(C') are high magnification: ((A) and (A'): 3MPa, (B) and (B'): 4MPa, (C) and (C'): 5MPa)

S11. Expansion ratio of the SIBS073T and SIBS062M stretching-induced foams

Figure S9 shows expansion ratios of the SIBS073T and 062M stretching-induced foams. Rectangular-shaped solid and foam samples were cut and expansion ratios of the stretching-induced were calculated by Eq. (S2-7) [9]:

$$Expansion\ ratio = \frac{\rho_s}{\rho_f} \qquad \text{(S11-1)}$$

where ρ_s is density of solid samples and ρ_f is density of foam samples.

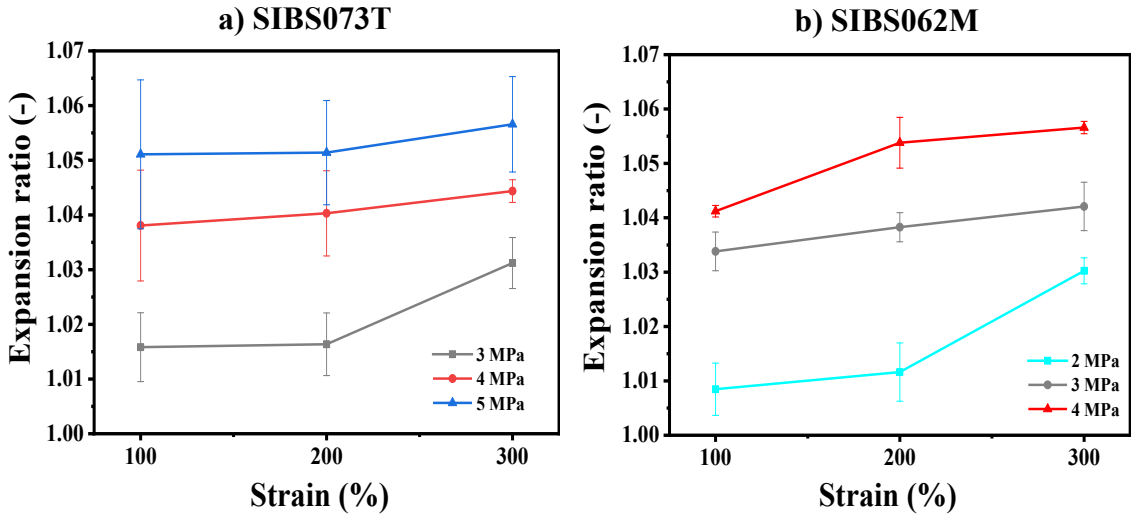

Figure S9. Expansion ratio of the SIBS073T and 062M stretching-induced foams.

S12. Stretching-induced foaming of SIBS073T with N_2

N_2-laden SIBS073T was prepared by the foam injection molding machine (SOFIT) and then stretched by the tensile tester. Immediately after injection molding, the N_2-laden elastomer was brought to the tensile tester to carry out the stretching-induced foaming with 300 % strain at four stretching rates, 0, 40, 200, and 400 mm/s. Instead of using CO_2 as a blowing agent, nitrogen, N_2 (Izumi Sanyo, Tokyo, Japan) was used as a

physical blowing agent (PBA). The other injection molding parameters are shown in Table S2.

Table S3. Experimental condition for preparing N_2-laden SIBS by the injection molding process.

Parameters	Values
Gas type	N_2
Gas pressure (MPa)	4
Cylinder Temperature (hopper to nozzle) (℃)	40, 120, 180, 200, 200, 200, 200, 200
Mold temperature (℃)	30
Holding pressure (MPa)	30
Injection speed (mm/s)	20
Dwelling time (s)	6

Figure S10 shows SEM images of the stretching-induced foams at different stretching rates. large bubbles were observed in the unstretched SIBS, similar to CO_2-laden SIBS discussed in main text. As shown in Figure S10, when the contents of PBA became higher, bubble nucleation occurred without stretching. However, the number of bubbles nucleated is less. When the number of bubbles reduces, the size of each bubble becomes larger because the amount of PBA consumable by each bubble increases, and bubble growth is enhanced. To prepare the N_2-laden sample without foaming, the temperature of the injected polymer or the PBA delivery pressure should be lowered. Comparing the SEM images of the same magnification, it is observed that the number of bubbles increased, and the size of the bubble decreased with the increased stretching rates. Figure S11 shows that the average bubble densities and size of the stretching-induced

foam indicated that stretching at a higher rate could promote bubble nucleation, even in the case of N_2.

Unstretched N_2-laden samples

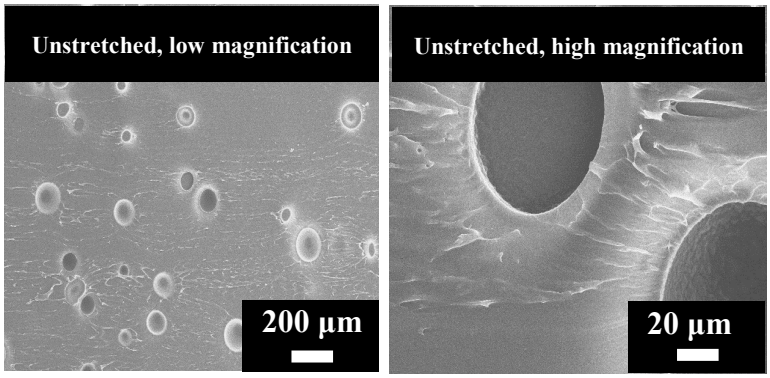

Stretching-induced foam at different stretching rates
(50, 200 and 400 mm/min) with a strain of 300% (4MPa N_2)

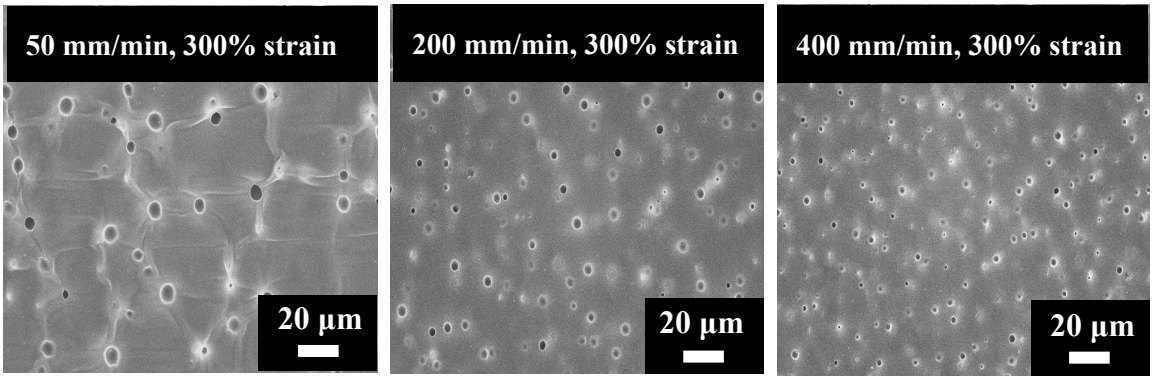

Figure S10 SEM images of the stretching-induced N_2-laden SIBS products at different stretching rates (0, 50, 200, and 400 mm/s)

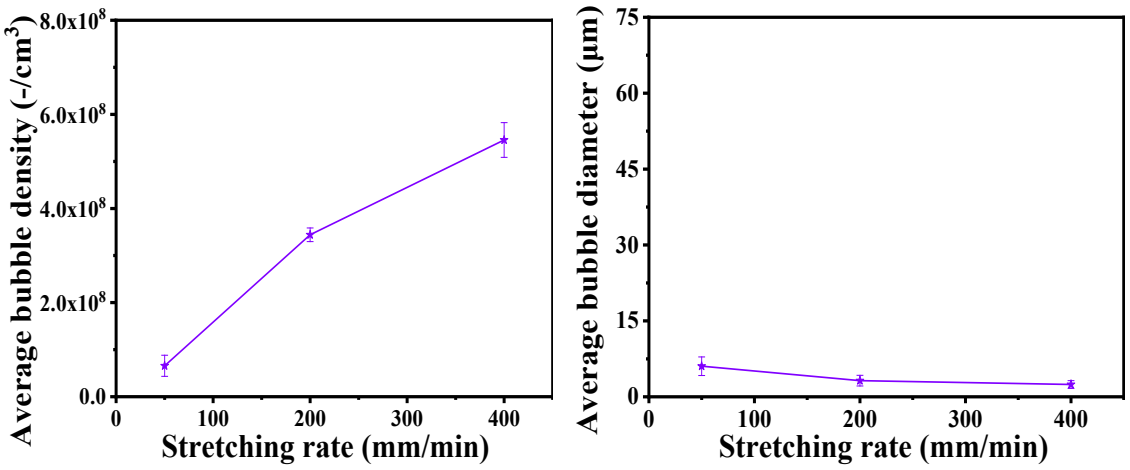

Figure S11. Bubble density and diameter of the stretching-induced SIBS073T-N_2 foams prepared with 4 MPa N_2 at different stretching rates (300% strain).

S13. Stretching-induced foaming of TPU with N_2

In addition to SIBS, a thermoplastic polyurethane, TPU (ET385, Elastollan®, BASF, Germany), was used to confirm the effect of stretching on the bubble nucleation in other elastomers. N_2-laden TPU samples were prepared by the same injection molding machine (SOFIT). Table S3 shows the experimental condition for preparing N_2-laden TPU by the injection molding process. Immediately after the injection molding, the N_2-laden TPU was brought to the tensile tester and stretched with 300 % strain at four stretching rates, 0, 40, 200, and 400 mm/s.

Figure S12 shows SEM images of the stretching-induced TPU foams at different stretching rates. Figure S13 summarizes the bubble density and size of the stretch-induced TPU foams. The cell structures of the stretching-induced foaming of TPU were similar to those of N_2-laden SIBS and CO_2-laden SIBS: Some bubbles were nucleated even in unstretching conditions, but the number of bubbles increased with the increased stretching

rates. The experimental results of N_2-laden SIBSs and TPU indicated that stretching promoted bubble nucleation in the physical foaming of elastomers, and the high stretching rate increased the number of nucleated bubbles and reduces the bubble size.

Table S4. Experimental condition for preparing N_2 -laden TPU by the injection molding process.

Parameters	Values
Gas type	N_2
Gas pressure (MPa)	5
Cylinder Temperature (hopper to nozzle) (℃)	50, 170, 180, 190, 200, 200, 200, 200
Mold temperature (℃)	30
Holding pressure (MPa)	30
Injection speed (mm/s)	20
Dwelling time (s)	6

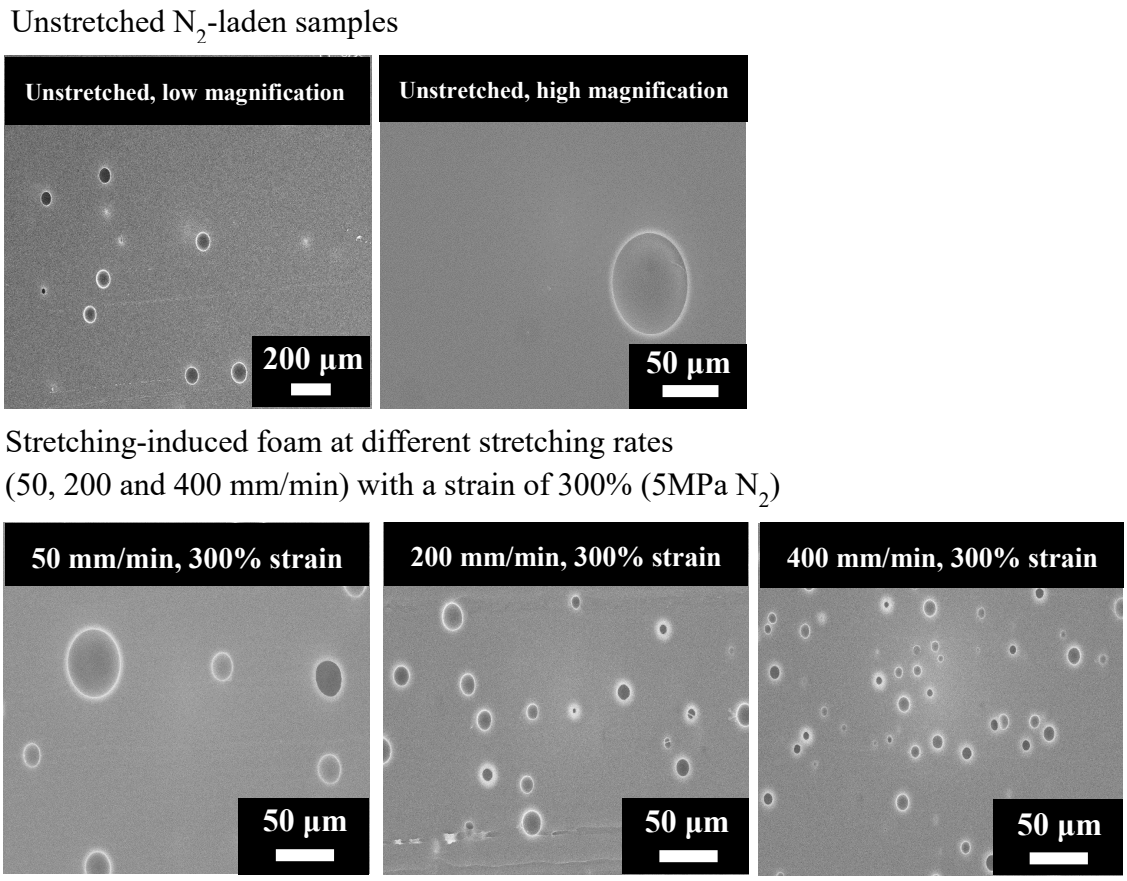

Figure S12. SEM images of the stretching-induced N_2-laden TPU at different stretching rates (0, 50, 200, and 400 mm/s)

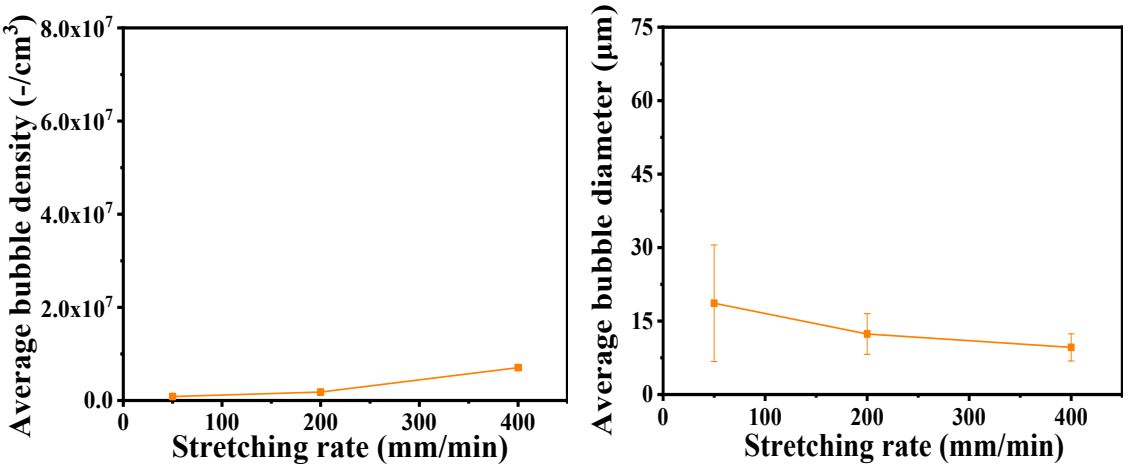

Figure S13. Bubble density and diameter of the stretching-induced TPU foams prepared with 5 MPa N_2 at different stretching rates (300% strain).

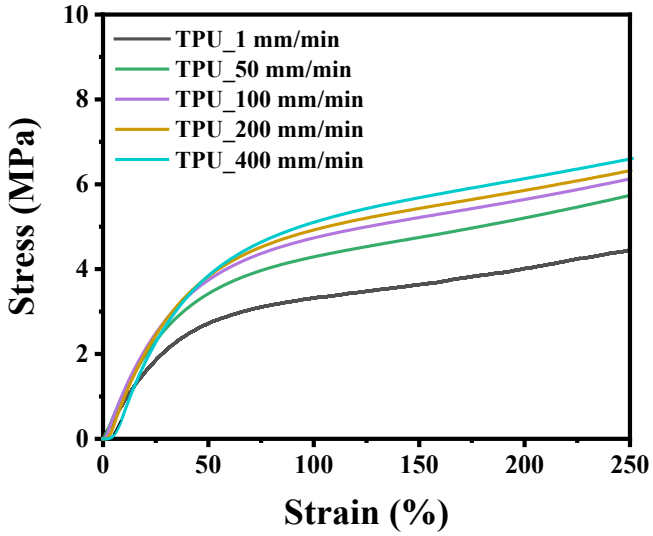

Figure S16. Strain–stress (S–S) curves of quasi-static and dynamic tests of TPU solid samples.

Table S5. Estimated parameter values from quasi-static and dynamic tensile tests of TPU.

Parameters	**TPU**
A_1 (MPa)	4.41
A_2 (MPa·s^n)	-4.52×10^{-1}
B_1 (MPa)	8.91
B_2 (MPa·s^n)	5.70×10^{-1}
Δg_{eb} in quasi-static test (MPa)	3.61×10^{-3}
n	0.31
Yield strain in quasi-static test (%)	2.86
Poisson's ratio	0.49

S14. Possibility of occurrence of SIBS073T strain-induced crystallization

DSC measurements were carried out by a Differential Scanning Calorimetry (DSC7020, Hitachi, Tokyo, Japan) at heating rate and cooling rate of 10 °C/min. The temperature was changed in the range from 30 to 200 °C. Figure S17 show the first heating and cooling curves of SIBS073T under different conditions: stretched solid samples with stretching rates of 50 and 400 mm/min, and 5 MPa unstretched sample.

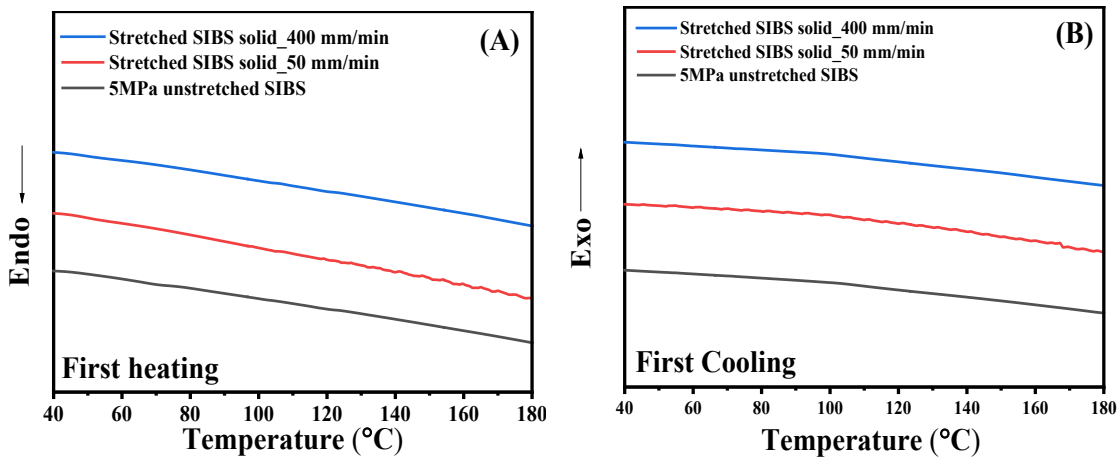

Figure S17. First heating curves and cooling curves of stretched SIBS073T samples: stretched solid samples with stretching rates of 50 and 400 mm/min, and unstretched sample (5 MPa).

References

[1] K. Yoshihashi, Industrial synthetic method of the rubbers 11. living radical (carbocationic) block-copolymer, *NIPPON GOMU KYOKAISHI* 2016, 89, 129-133.

[2] P. Gong, T. Taniguchi, M. Ohshima, Nanoporous structure of the cell walls of polycarbonate foams, *J. Mater. Sci.* 49 (2014) 2605–2617.

[3] G. Wang, J. Zhao, K, Yu, L. H. Mark, G. Wang, P. Gong, C. B. Park, G. Zhao, Role of elastic strain energy in cell nucleation of polymer foaming and its application for fabricating sub-microcellular TPU microfilms, *Polymer* 119 (2017) 28–39.

[4] N. H. Kim, B. V. Sankar, and A. V. Kumar, *Introduction to Finite Element Analysis and Design, 2nd Edition*, John Wiley &Sons Ltd.: New Jersey, 2018.

[5] I. M. Ward, Review: The yield behaviour of polymers, *J. Mater. Sci*. 6 (1971) 1397–1417.

[6] J. Yu, Q. Fei, P. Zhang, Y. Li, D. Zhang, F. Guo, An innovative yield criterion considering strain rates based on von Mises stress, *J. Press. Vessel Technol.* 142 (2020) 014501-1–014501-6.

[7] X. Du, Q. Zhang, Z. Wan, A nonlinear constitutive model for rayon-rubber composite in the medium strain rate range, *J. Elastomers Plast.* 27 (1995) 91–99.

[8] A. F. Bower, *Applied Mechanics of Solid – Chapter 3 Constitutive Models: Relations between Stress and Strain*; CRC Press: Boca Raton, 2009.

[9] C. Yang, G. Wang, J. Zhao, G. Zhao, A. Zhang, Lightweight and strong glass fiber reinforced polypropylene composite foams achieved by mold-opening microcellular injection molding, *J. Mater. Res. Technol*. 14 (2021) 2920–2931.